

HEATED FRICTION STIR WELDING: AN INVESTIGATION INTO HOW  
PREHEATING ALUMINUM 6061 AFFECTS PROCESS FORCES

By

Paul Sinclair

Thesis

Submitted to the Faculty of the  
Graduate School of Vanderbilt University  
in partial fulfillment of the requirements  
for the degree of

MASTER OF SCIENCE

in

Mechanical Engineering

May, 2009

Nashville, Tennessee

Approved:

Professor Alvin M. Strauss

Professor George E. Cook

Professor David R. DeLapp

## ACKNOWLEDGEMENTS

I would like to take this opportunity to thank those who have given me so much support during the last two years. My research advisors, Drs. Al Strauss, George E. Cook, and David De Lapp; lab mates Paul Fleming, David Lammlein, Russel Longhurst, Tracie Prater, Thomas Bloodworth, Chase Cox, and Chris Hendrix; The Vanderbilt Physics Department Machine Shop for design and machining work; The NASA Space Grant for providing financial support through the project; my family and friends who have supported me being here; and the Rhodes College Physics Department for allowing me to get here.

# TABLE OF CONTENTS

	Page
ACKNOWLEDGEMENTS.....	ii
LIST OF TABLES.....	v
LIST OF FIGURES.....	vi
Chapter	
I. INTRODUCTION.....	1
II. LITERATURE REVIEW.....	7
III. EXPERIMENTAL METHOD.....	12
3.1 Overview of Vanderbilt’s Friction Stir Welding Machine.....	12
3.2 The Heating and Thermal Insulation Systems.....	17
3.3 The Backing Plate and Clamping System.....	19
3.4 Trivex FSW Tool.....	21
3.5 Position Control Welding Process.....	23
3.6 Force Control Welding Process.....	27
3.7 Post-weld analysis: Forces.....	29
3.8 Post-weld Analysis: Metallography.....	30
IV. RESULTS.....	31
4.1 Position Control Weld Results.....	31
4.2 Force Control Weld Results.....	37
4.3 The Backing Plate and Clamping System.....	19
V. DISCUSSION.....	42
5.1 The Reduction in Axial Forces.....	42
5.2 Discussion of the Average Welding Torque.....	43
5.3 Fixing the Weld Defects.....	44
5.4 FLUENT CFD Modeling of Heated FSW with a Trivex Tool.....	45
5.5 Conclusions and Future Work.....	50

Appendix

A. SOURCE CODE FOR THE TRAVERSE SPEED FORCE CONTROL PROGRAMMING .....	42
B. POSITION CONTROL WELD AXIAL FORCE PLOTS.....	43
REFERENCES .....	69



## LIST OF TABLES

Table	Page
1. Temperature Dependency of Aluminum AA 6061-T6 Yield Strength .....	7
2. Comparison of Thermal Insulation Materials .....	18
3. Position Control Weld Matrix.....	26
4. Force Control Weld Matrix.....	28

## LIST OF FIGURES

Figure	Page
1. Schematic of Typical FSW Process .....	1
2. FSW Tools .....	2
3. Schematic of a Typical FSW Cross-Section.....	4
4. A Simplified Diagram of Arc-Enhanced FSW .....	8
5. A FSW Setup with Induction Heating .....	9
6. A FSW Setup with an Electric Heating Element .....	10
7. Tensile Strength Comparison of Different Heated Welds .....	11
8. Vanderbilt University Welding Automation Laboratory's FSW Machine.....	13
9. The Lower Spindle.....	14
10. FSW Machine Motors.....	16
11. The Raised Anvil Assembly Drawn in CAD.....	20
12. The Heating and Welding System Drawn in CAD.....	20
13. Heated FSW System .....	21
14. The Trivex Tool CAD Design .....	23
15. The Weld Controller Program GUI .....	24
16. Weld E11, Axial Force (N) vs. Time (s).....	31
17. The Rising Trend in the Axial Force Graph for Weld C05 .....	32
18. Average Axial Forces for the Position Control Welds .....	33
19. Normalized Axial Forces for the Position Control Welds .....	34
20. Average Torque and Power Values for the Position Control Welds .....	35

21. Normalized Axial Forces for Heated Welds at Various Travel Speeds.....	35
22. Macrosections of the 11 ipm Welds.....	36
23. The Connection Between the Two Defects .....	37
24. Individual Force Control Weld Graphs.....	38-40
25. Average Force Control Weld Results .....	41
26. Detail of the Trivex Pin Model Elements .....	47
27. FLUENT Model Thermal Boundary Conditions.....	48
28. FLUENT Material Flow Vectors .....	48
29. FLUENT's Axial Forces for Varying Initial Weld Temperatures.....	49
30. Average Torque and Power Values for the Position Control Welds .....	35
31. Average Torque and Power Values for the Position Control Welds .....	35

# CHAPTER I

## INTRODUCTION

Developed in the early 1990's in the United Kingdom by The Welding Institute (TWI) [1], Friction Stir Welding (FSW) is a solid-state joining process now used and researched around the world. During a weld a rotating cylindrical tool is driven through the material to be welded, heating the material to a plasticized state and literally stirring the work pieces together. While initially performed in aluminum FSW is now achieved in a variety of materials and joint configurations. It offers numerous benefits over conventional forms of welding and with continued work is being applied to an ever-growing number of projects and situations.

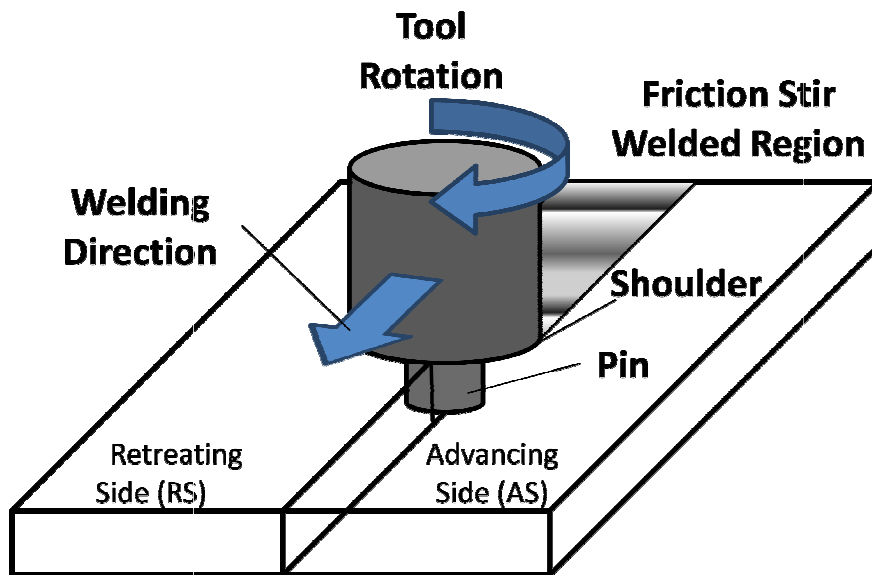


Figure 1 Schematic of Typical FSW Process

Figure 1 shows a typical FSW arrangement. In traditional FSW, the cylindrical tool is driven at an angular velocity  $\omega$  (rpm or rad/sec) and plunged into the work piece. The horizontal shoulder of the tool contacts the surface of the material while the lower pin is driven through it. Actual tools created for FSW are shown in Figure 2. Due to the friction between the tool and the work piece, significant heat is generated which brings the material immediately around the pin to a plasticized state. The tool is driven along the weld joint at a feed rate  $f_r$  (in/min, ipm, or mm/sec), and through the action of the tool the work undergoes severe plastic deformation: it is effectually stirred together to create the weld. The side of the weld where the tangential velocity and welding direction are parallel is referred to as the advancing side (AS) of the weld; the other side where the vectors point in opposite directions is called the retreating side (RS). In general FSW is a stable process: as the temperature of the material around the tool rises, the frictional forces and thus heat input decrease. As the environment near the tool cools, additional heat is generated by increased friction.

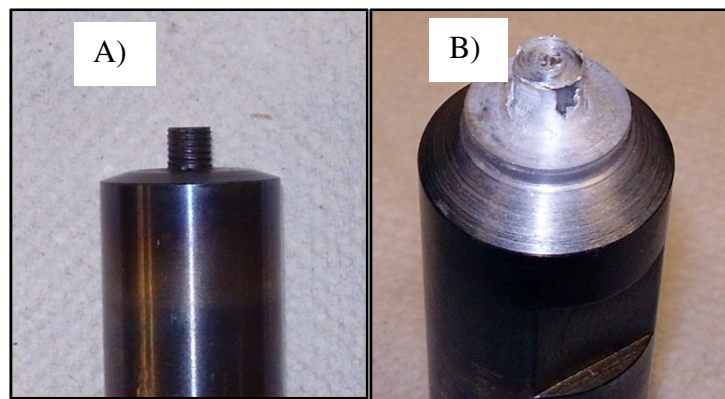


Figure 2 FSW Tools (A) A new .250" diameter threaded pin tool.  
(B) A Trivex<sup>TM</sup> tool after several welds through AA 6061 Aluminum.

Two of the major independent variables in FSW are those just mentioned: the rotational speed  $\omega$  and the travel speed  $f_r$ . These are often considered together as the

weld pitch: the ratio of  $f_r$  to  $\omega$ . The weld pitch's affect on material flow has been compared to the influence of cutting speed on chip formation in machining processes. A lower weld pitch (less forward travel per revolution of the FSW tool) leads to more continuous flows and better welds, similar to how increased cutting speeds lead to more continuous machining chips [2]. Of course, a lower weld pitch also means the weld takes longer to complete.

The tool's positioning relative to the work piece defines another group of important parameters: the plunge depth, which is the vertical position of the tool's shoulder, and the tilt angle, which is the angle of between the tool's axis and the vertical. The final major independent variable set is of course the tool itself: its size, shape, and features. These variables work together to influence the thermal and flow patterns within the weld, and much of FSW research and industrial development is devoted to optimizing these parameters for specific situations.

Of course, a range of dependant variables are measured corresponding to the domain presented above. During the FSW process, the most commonly recorded variables are the welding forces. The three orthogonal forces relative to the work piece are recorded:  $F_x$  is the translational force,  $F_y$  is the traverse force, and  $F_z$  is the axial force. The moment about the z axis is also frequently recorded. After the weld is completed its quality and strength are analyzed using any number of joint strength measures, from non-destructive optical and ultrasound inspection to destructive tensile and bending tests. Joint efficiency – a measure of the strength of the welded joint compared to the parent material - is an important measure especially in industry. Under optimal FSW conditions joint efficiencies approach 100% [3]

It is also very common to study etched metallurgical cross-sections of friction stir welds. There are four noticeable regions created by the FSW tool separated by how much heat and deformation the material was exposed to. In the center where the pin has passed is the weld nugget, characterized by the greatest deformation and as a site of recrystallization. Surrounding the nugget is the thermal mechanically affected zone (TMAZ), which contains grains of the original material in a deformed state. The third layer, affected by the heat of the weld but lacking the deformation of the more central zones, is referred to as the heat affected zone (HAZ), similar to conventional fusion welding. Finally, the unaffected original material is often called the parent material or the unaffected zone; both names are relatively descriptive. Figure 3 shows a schematic cross section of these four zones in a typical FSW arrangement. The asymmetrical nature of the nugget and surrounding zones is a result of differing flows between the AS and RS of the weld.

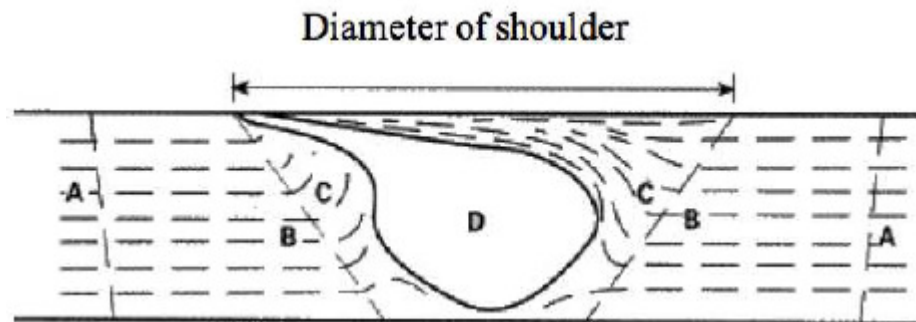


Figure 3 Schematic of a typical FSW Cross-Section (A) Parent Material. (B) Heat Affected Zone. (C) Thermal Mechanically Affected Zone. (D) Weld Nugget [4]

FSW offers a number of advantages over conventional fusion welding techniques. FSW can be used with materials and alloys considered hard or impossible to weld by conventional means; it can also join different materials and different thicknesses of

materials. With the proper parameters it offers less distortion, improved weld quality, and faster welding speeds all the while requiring less operator skill. FSW tools are generally very robust, welding great distances before wearing out, which combined with the absence of needed filler or flux material means there are nearly zero consumables. Finally, this new welding scheme generates no fumes or requires any shielding gasses, and because of the lower level of heating it requires less overall energy than any fusion welding. All of these advantages and efficiencies add together to make FSW a very “green” process, a fact that is not lost on industry in today’s age [5-7].

Due in large part to its many advantages, FSW has grown rapidly in the material joining community since its introduction. Nearly all imaginable types of joint configurations are now being welded. As the heating and flow mechanisms are slowly understood, the tools have grown increasingly advanced and able to weld more material with less forces and tool wear [7]. Probably the most important growth has been in the selection of materials being welded. The field started out welding aluminum and its alloys with tools made out of steel. Once good parameters were found the tools produced robust welds with manageable forces and long tool life. Other softer metals including copper and magnesium have also successfully undergone FSW with relative ease.

There is pressure from many industries – especially transportation, space, oil and gas transport, and defense – to friction stir weld higher strength materials, specifically the various steel and titanium alloys. And indeed, this has been done very successfully, but the strength of these materials generates much higher welding temperatures, easily reaching 1100 °C and higher. These temperatures are accompanied by much higher welding forces, and the environment has resulted in vastly accelerated tool wear [2, 7].



The general response of the FSW community to the problem has been to create tougher tools: going to refractory alloys such as tungsten-rhenium (W-Re) and tungsten-carbide (W-C) or ceramics such as polycrystalline cubic boron nitride (PCBN). These tools have produced sound welds in steel and titanium alloys, but certainly drive up the cost and difficulty of the FSW process [8].

The problems with higher strength material FSW has also prompted a look into how to reduce the forces experienced by the tool in a general sense. Reducing the forces required to perform FSW has a number of sought-after benefits: reduced tool wear, faster travel speeds, smaller clamping forces, less wear on the welding system, and less energy consumption. One way this is accomplished is with more advanced tool designs, such as the development of the Trivex pin by TWI [9]. Alternatively, a material's strength characteristics generally fall as it is heated – indeed, this is the one of the basics of FSW. By finding additional ways to heat up the material being welded in front of the tool the initial material temperature for the FSW process is increased, therefore reducing the heat input required from the tool and thus the frictional loads [2]. Exploring the potential advantages of this initial welding temperature is the focus of the following investigation.

## CHAPTER II

### LITERATURE REVIEW

Nearly all materials lose strength as they are heated; indeed, this is one reason that FSW tools are able to “stir” the material together once the frictional forces have raised the local temperatures. Table 1 shows how the yield strength of Aluminum 6061-T6 depends on the material’s temperature.

Table 1 Temperature Dependency of  
Aluminum AA 6061-T6  
Yield Strength [10]

Temperature (K)	Yield Strength (MPa)
311	241
339	238
366	232
394	223
422	189
450	138
477	92
533	34
589	19
644	12

In usual FSW the tool is responsible for all heat input to the weld. Theoretical models generally consider the heat contribution from the shoulder and pin as separate heat sources and attribute 80% or more of the heating as coming from the shoulder [2, 7, 10].

However, if an additional source of heating is introduced the heat input required from the FSW tool is obviously reduced. This is a point touched on by many authors but rarely dealt with in earnest. One common way to implement another heat source is to attach some other welding instrument, often some sort of under-powered fusion welding tool, just in front of the FSW tool. This approach is often termed “hybrid-“ or “assisted-FSW”. Oak Ridge National Lab has added a laser welding system to FSW and reported seeing 50% drops in the welding forces [11]. Several patents have issued on other laser-assisted FSW processes and improvements [12]. Another patent claims a similar pre-heating system, this time with a TIG arc-welding torch, which reduces FSW tool wear, extends the range of FSW to harder materials, and helps join dissimilar metals [13].

Figure 4 shows a diagram of this arc-enhanced FSW.

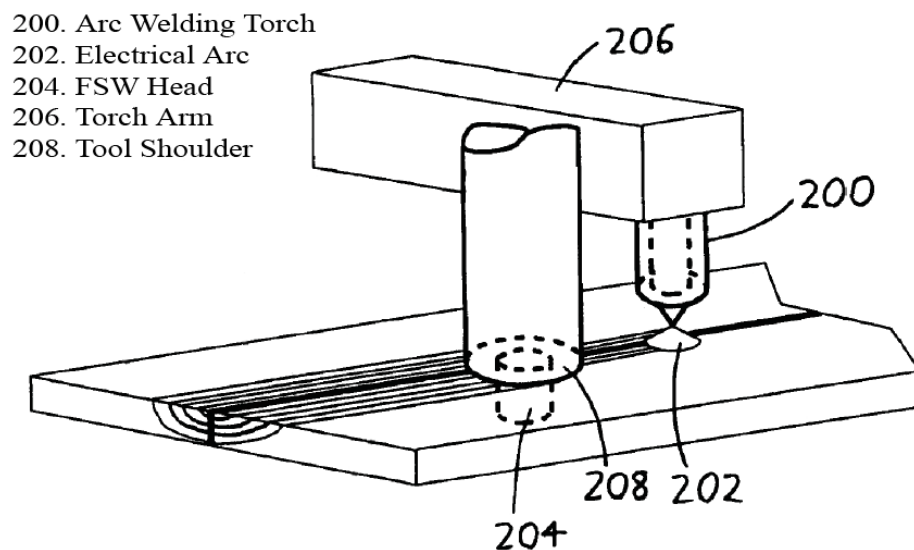


Figure 4 A Simplified Diagram of Arc-Enhanced FSW [13]

Another assisted-FSW system was constructed by Grant et al. [14] to help weld in cast iron. Even when using W-Re and PCBN tools tool wear became a major problem.

The authors implemented an induction heating system in front of the FSW tool to warm the iron with induction heating. Like the other systems the induction coil traveled just in front of the FSW tool, heating the material and reducing the process loads on the tool itself. The authors' setup can be seen in Figure 5. The system realized great reductions in the X and Y tool forces. However, there was no indication of the temperature the heating system achieved or the distribution of that temperature within the work piece. Further, this induction system will work only with magnetic welding materials.

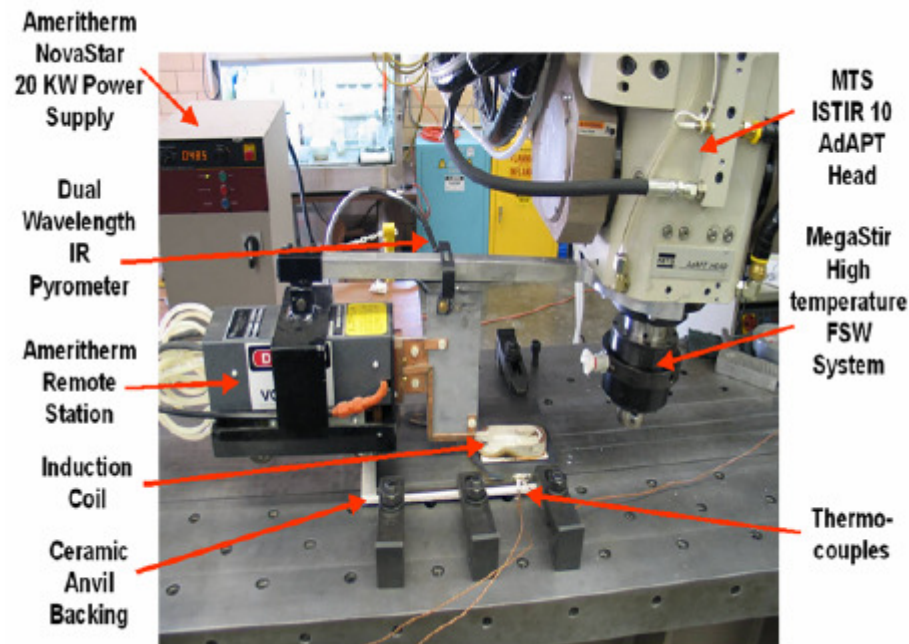


Figure 5 A FSW Setup with Induction Heating [14]

Probably the most precise heating data in the FSW literature to date comes from Riichi et al. [15]. This group studied the feasibility of FSW pre-heated aluminum by studying the cross sections and tensile strength of welds in 5052-H34 aluminum after heating to 150, 200, 300, 350, and 400 °C. The preheating was done by placing a large electric heating element within the backing anvil of the system and insulating the weld

specimen from the clamping system. A general diagram of this set-up is shown in Figure 6.

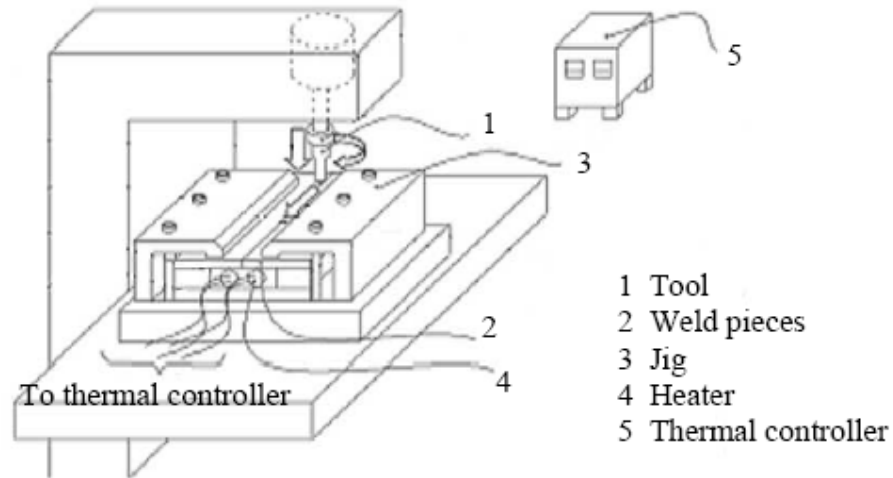


Figure 6 A FSW Setup with an Electric Heating Element [15]

This paper concludes that FSW with heating is indeed feasible although their 350 and 400 °C welds showed definite signs of excessive heat input. Perhaps more importantly Riichi et al. showed that there was very little effect on the tensile strength of the welds, as seen in Figure 7. Unfortunately the authors did not measure the FSW processing forces.

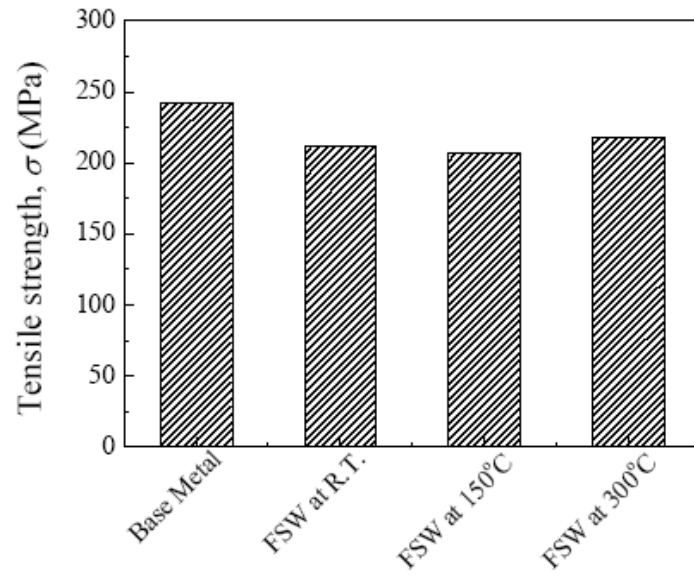


Figure 7 Tensile Strength Comparison of Different Heated Welds [15]

## CHAPTER III

### EXPERIMENTAL METHODS

#### 3.1 Overview of Vanderbilt's Friction Stir Welding Machine

The overall goal of the experiments herein described was to describe the effects manipulating the initial temperature of the work piece in FSW. The following describes the welding apparatus and procedure used in the experiments, the acquisition and analysis of the weld data, and the post-weld microscopy procedures.

The Welding Automation Laboratory at Vanderbilt University uses a modified Milwaukee #2K Universal Horizontal Milling Machine for FSW. The machine features a Heavy Duty Kearney and Trecker Vertical Head Attachment with a vertical spindle. The spindle head is capable of very small rotations about the y-axis, used to establish the tilt angle desired for welding. The spindle itself is driven by a Baldor Industrial VM 2514, 20 horsepower, 3-phase 230VAC motor rated for rotational speeds of 3450 RPM. The driving mechanism is a poly-v belt and pulley system; as the driver pulley (Emerson/Browning/Morse part 16J45P) measures 4.5 inches in diameter, and the driven pulley (16J60P) is 6.0 inches in diameter, the actual spindle head is under-driven by a 7:12 ratio. This results in an increase in available torque but a decrease in the maximum RPM to approximately 2100. A labeled front view of the entire machine is shown in Figure 8.

The spindle head bearings are lubricated by a bijor oil-mist system during the weld cycle, which is computer-controlled to start at the beginning of each weld cycle. The lubricant itself is DTE Light Bearing and Circulating Oil #ISO VG 32. Nitrogen gas

is used to pressure the lubricant through the delivery tubing and into the bearing housings. These delivery lines can be seen to the left of the spindle head in Figure 8.

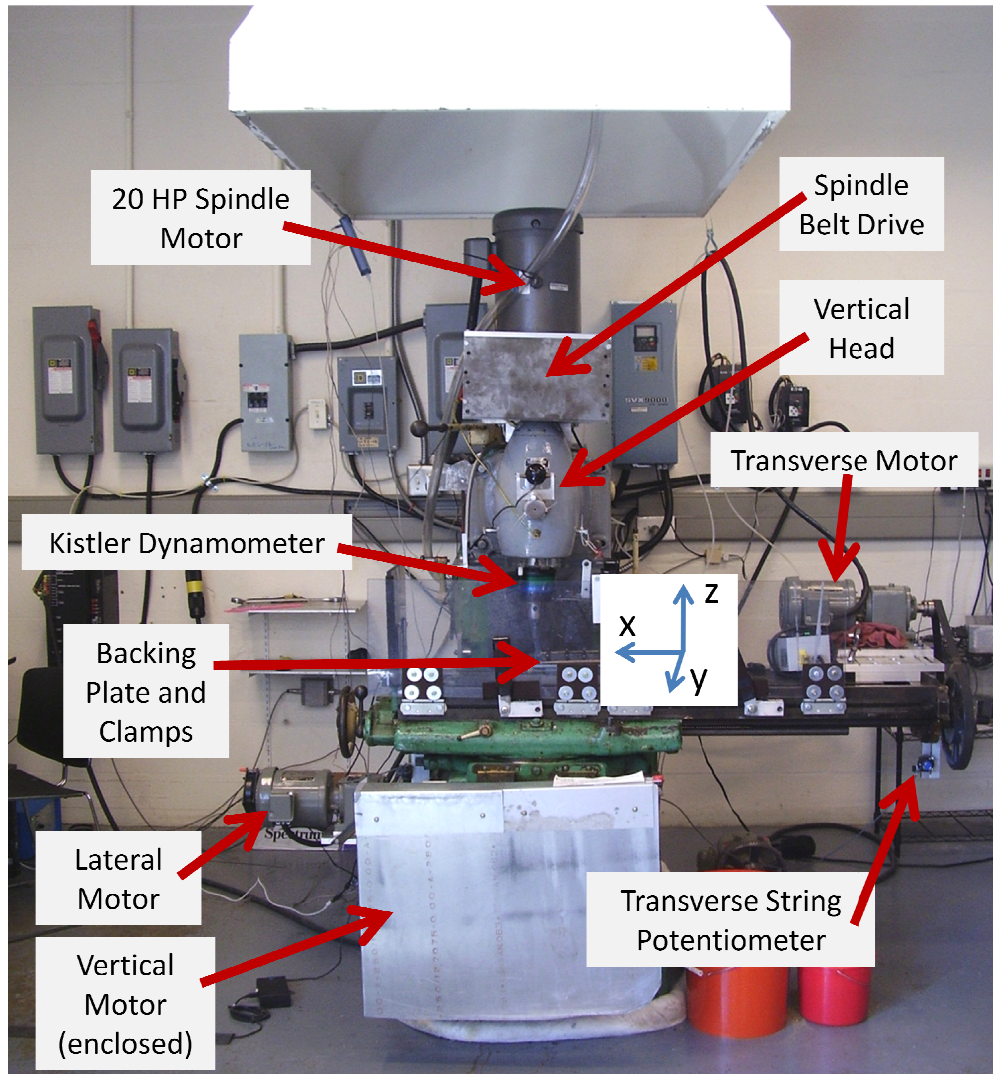


Figure 8 Vanderbilt University Welding Automation Laboratory's FSW Machine

The blue and green cylindrical instrument just underneath the vertical head is, as indicated in Figure 8, the Kistler Rotating Cutting Force Dynamometer. This unit records forces in all three directions as well as the torque. Unfortunately the x and y axis forces are coupled with the dynamometer itself; that is they rotate with the tool during the weld.



To compensate this, the base of the dynamometer is fitted with two optical encoders, as shown in Figure 9. The optical encoders consist of a small laser and optical sensor. The pictured brass fins work to block the laser's path, and the optical encoder transmits a signal each time it goes from blocked to un-blocked. The lower interrupter features ten fins evenly distributed every 36 degrees. The dynamometer data is poled on each interruption, giving ten data points per revolution. The higher interrupter features only one fin approximately 18 degrees wide and works to count the actual revolutions of the spindle as well as establish a zero location for the lower encoder's data.

The second limitation of the Kistler dynamometer is its maximum safe operating temperature of 60 °C. As heat naturally escapes the weld through convection in the tool and up into the spindle, this temperature bound limits the Vanderbilt lab to welding materials with lower melting temperatures such as aluminum and magnesium.

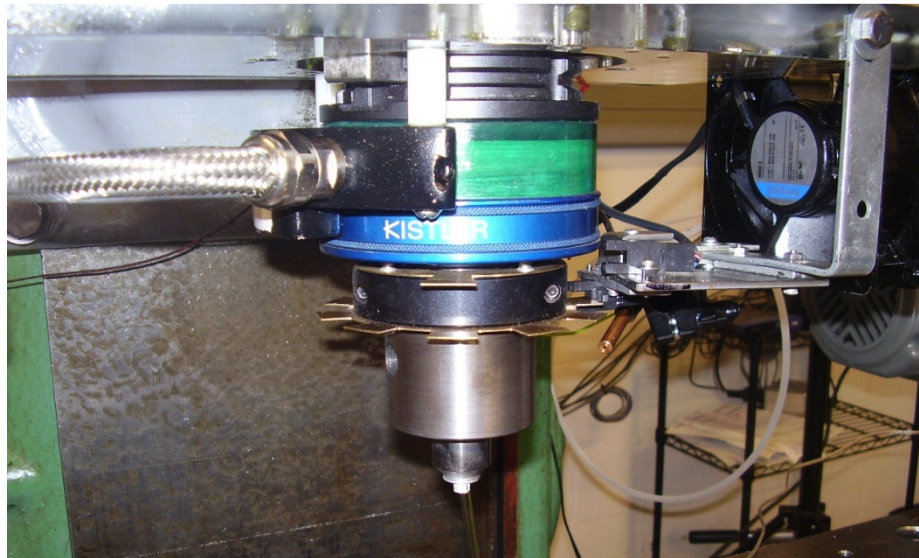


Figure 9 The Lower Spindle. Shows the Kistler dynamometer and optical encoder set-up.

Just below the dynamometer is the chuck for the FSW tool. This is a 3 inch diameter steel cylinder is securely bolted to the dynamometer with four grade-8 bolts.

The inner hole of the mount accepts 1.000 inch diameter tools with a very slight clearance fit. All FSW tools made for the Vanderbilt welding lab feature a flat indentation ( $\frac{1}{2}$ " x  $\frac{1}{2}$ " x .100") milled into the upper portion of the tool, allowing the tool to be keyed to the mount with a set-screw, seen on the left side in Figure 9. A second setscrew is tightened against the first to lock in place. This mounting system ensures that the tool will not deflect or slip during the course of the weld.

The Milwaukee #2K Milling Machine's table feed has been heavily modified to provide for computer control along all three axes. This automation provides much greater reliability and precision in the welding process. Three external motors power the table while a series of sensors provide feedback. The lateral and traverse axes – the y-axis across the weld and the x-axis along the weld, respectively – are powered by U.S. Electric 1 horsepower type TF GDY TE frequency-drive motors. The lateral gear train has ratio of 6.02, which combined with the minimum driving frequency gives a speed range between 1.7 and 8 ipm. The table is equipped with a string potentiometer which provides absolute position information to the controlling computer. It also features an optical encoder with measurement of relative precision; this secondary encoder is normally used in joint tracking experiments where increased position resolution is necessary. The traverse motor has the same specifications as the lateral but with the inclusion of a 5.25:1 ratio belt drive. This gives a maximum traverse speed to 14 ipm, a reasonable figure for weld traverse speeds; if higher travel speeds are needed the gear train and belt drive ratios can be changed. Another string potentiometer is used to provide the absolute position of the traverse axis position to the computer.

The vertical motor and drive train is located in front of the machine, enclosed in a metal shield to protect the machine's users. The position of the FSW tool within the weld is incredibly important; to allow for finer control the vertical axis is driven by a Parker Compumotor servo motor, model number 730 MTR. The drive train for this motor provides for a maximum vertical velocity of 5 ipm; the nature of the servo motor allows for fine control in exceptionally small travel increments. A magnetic sensor strip with a zero position is mounted on the side of the machine and reads the absolute vertical position of the table. The lateral, transverse, and vertical motors and gear trains are pictured in Figure 10.

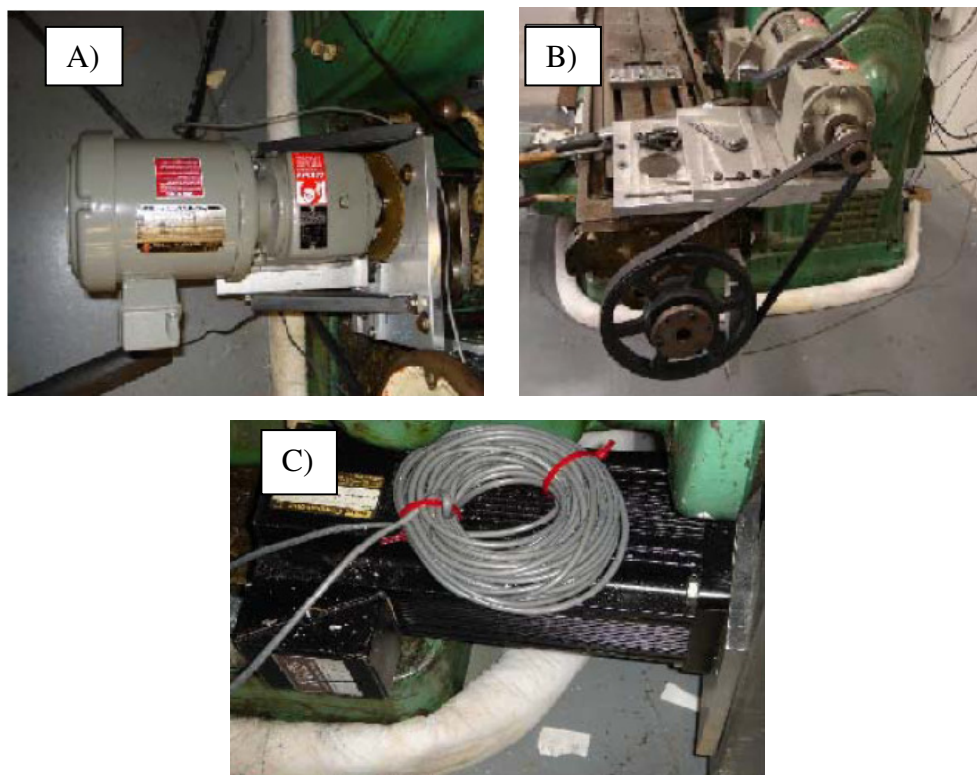


Figure 10 FSW Machine Motors (A) The lateral motor and drive head. (B) The traverse motor and drive train. (C) The vertical stepper motor

### 3.2 The Heating and Thermal Insulation Systems

Two heating elements were employed to heat the aluminum samples up to the desired temperatures. The first of these was a BriskHeat Wide Fiberglass Heavy Insulated heating strip, part number BIH251020L. This flexible fiberglass-knitted tape is 2.5" x 24" and approximately ¼ inch thick. Inside the strip are two heating elements which run parallel down the strip and together produce 313 total watts of heating or approximately 5.1 watts/in<sup>2</sup>. This heating element was used for the initial system design and first welds.

The fiberglass heating strip was able to heat the system to about 100 °C: at this point the heat loss from the aluminum was equal to the heat input the flexible strip could provide. Once a few welds were completed, it was obvious the heating element did not need flexibility and achieving higher material temperatures was desirable. To create these higher initial material temperatures a high temperature mica heating strip was acquired. ProTherm Industries part number PRT15985 is a ceramic heating strip measuring 2.5" x 11" which produces 1600 total watts, or approximately 58 watts/in<sup>2</sup>. The mica heating strip was easily able to heat the system past the 300 °C welds that formed the upper end of the weld matrix.

Both heating elements worked with the BriskHeat TTD999-K120 Thermocouple Controller. This unit implements a very basic feedback control. A thin 1" square type-K thermocouple was put on top of the heating element, and a desired temperature was set in the controller. Like a simple thermostat, the controller turns the heating element on if the measured temperature is below the input, and turns it off when the measured temperature is above the desired level. Despite this fairly simple regulation, the initial material temperatures were always within ±2 °C of the desired value.

Once the heating system was assembled, tests showed that the system worked best when placed just under the weld samples and thermally insulated from the surrounding materials. The lab had a small supply of G10 “Garolite” fiberglass laminate which is known for its low thermal conductivity and good strength characteristics. This material was used below the heating element and between the weld sample and the clamping system to very effectively minimize heat loss. The G10 was melting under the conditions of the hotter welds, and so the insulation material was switched to the higher-temperature G7 Glass-Silicone laminate. Table 2 shows a comparison of the two insulation material properties. To help further protect the insulation from the concentrated heating elements, a .125” piece of aluminum was put between the heating element and the insulation to spread the thermal energy across the whole area.

Table 2 Comparison of Thermal Insulation Materials [16]

	Substrate Material	Thermal Conductivity	Compressive Strength	Melting Temperature
Insulation		(W/m-K)	(MPa)	(°C)
G10	Fiberglass	.288	448	140
G7	Glass-Silicone	.288	345	220

### 3.3 The Backing Plate and Clamping System

The Vanderbilt FSW system features a precision-ground, cold-rolled steel backing plate of dimensions 24" x 7" x 1" which is bolted carefully and firmly to the milling machine's table. Due to the set-up process before welding, too much heat would be lost by conduction to this backing plate if the aluminum weld samples were heated separately from the welding set-up and then clamped down. Alternatively it was deemed impractical to attempt and heat the entire backing plate. A much smaller anvil was therefore constructed to cover and protect the heating element while providing a solid backing plate to weld on. This raised anvil would have a short, squat tunnel shape to it in order to cover and protect the heating element, withstand the welding process forces, and still be easily heated.

The software controlling the FSW machine, in order to help prevent damage, is programmed to stop the welding process if the axial force exceeds 15,000N. To withstand this force the top piece of the anvil was constructed from .250" thick precision-ground AISI 1006 mild steel. Quick calculations showed that, if simply supported over the 3" width of the heating element, under the FSW machine's greatest load this top piece would deflect less than .0002" while experiencing stresses less than 2/3 of the yield strength. The legs of the raised backing plate were also constructed from AISI precision-ground steel; these were 5/32" thick to equal the heating element and were screwed to the top piece. The whole anvil is 10" long and 4" total width and is shown in Figure 11.

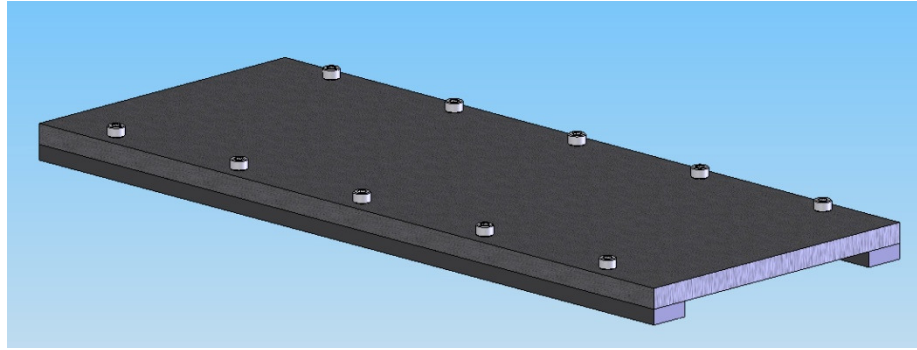


Figure 11 The Raised Anvil Assembly Drawn in CAD

With the raised anvil constructed, the heating and backing plate system was assembled. The large piece of thermal insulation was laid down on the original large backing plate, and the thin aluminum heat spreader placed on top of that. The heating element was placed centrally down on the heat spreader, and the raised anvil covered the heater. A thin K-type thermocouple, used to monitor the temperature of the heating element and steel, was slid approximately 1” under the anvil and on top of the heating element. Finally the aluminum weld sample was placed on the anvil, with the final two thin strips of insulation along its edges to insulate the clamping system. The entire assembly can be seen in Figure 12.

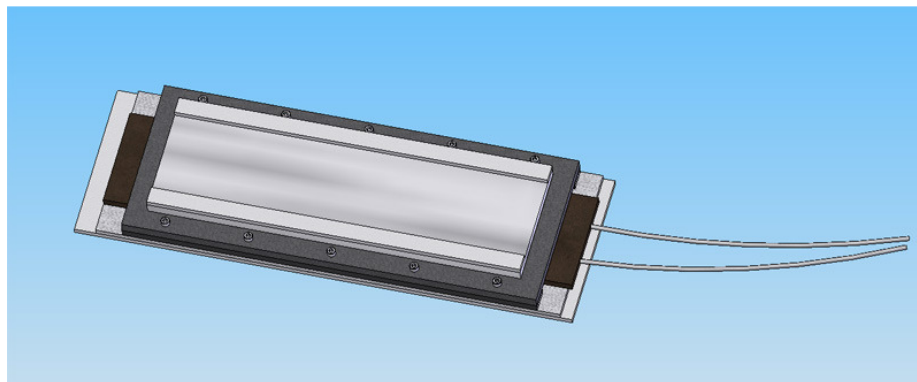


Figure 12 The Heating and Welding System Drawn in CAD

As the investigation concerned the FSW process forces and not the actual joint optimization or strength, all welds conducted were bead on plate welds where the tool passes through a solid piece of aluminum. The weld samples were plates of AA 6061-T6511 aluminum, nominally .250" thick. The samples were 3 inches wide and 9 inches long. To accurately measure the temperature of the aluminum prior to welding, two braided J-type thermocouples were embedded in the samples, one on the advancing side 2" from the start of the sample, and one on the retreating side 2" before the end. Each thermocouple hole was .600" deep. The samples were clamped in place with .250" thick pieces of steel coming in on each side; the clamps were located on threaded studs, balanced with thick shims on the outside, and secured with nuts tightened to about 25 ft-lbs. The welding set-up is pictured in Figure 13.

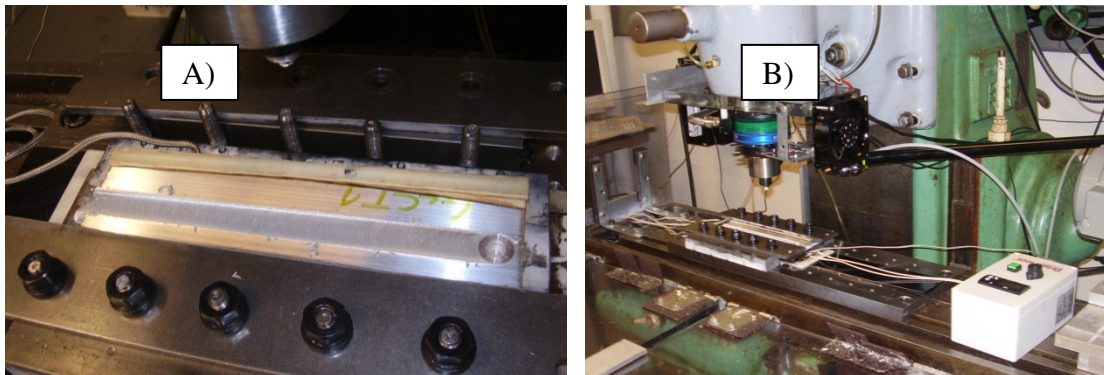


Figure 13 Heated FSW System (A) A picture of the anvil and clamping set-up with one clamp removed. One of the J-type braided thermocouples can be seen in the aluminum. (B) The entire welding set-up including the BriskHeat Thermocouple Controller.

### 3.4 Trivex FSW Tool

All the welds in this research were performed with a Trivex tool, a pin shape designed using computational fluid dynamics by Colegrove and Shercliff of TWI [9]. The Trivex tool design is approximately triangular; the three points of the tool form an



equilateral triangle and are connected by convex sides. Each vertex is the center of a circle containing the other two vertices. The CAD drawing used to make the tool used, showing the Trivex pin design, is in Figure 14. This tool was chosen for several reasons. First, the absence of pin features such as threads or flutes eliminates stress concentrations and thus helps prevent pin breakage. With many welds planned for the experiment, a robust tool design was very helpful. Secondly, the Trivex tool has been used often in the past by the Vanderbilt welding lab, so there were tools available to use and a body of knowledge about using them. Finally, the Trivex tool design is effective at reducing the FSW process forces, in line with the overall spirit of this investigation.

The tool was made of H-13 tool steel heat treated to Rc 48-50. Based on previous work the tool was put on a  $1^\circ$  tilt angle and set with a plunge depth of .0074" to achieve 80% shoulder contact. For this geometry and plunge depth, the pin was shortened to .237" to place the bottom corner of the pin just shy of .01" above the raised backing plate. This distance gives a full penetration weld without risking welding the aluminum to the steel.

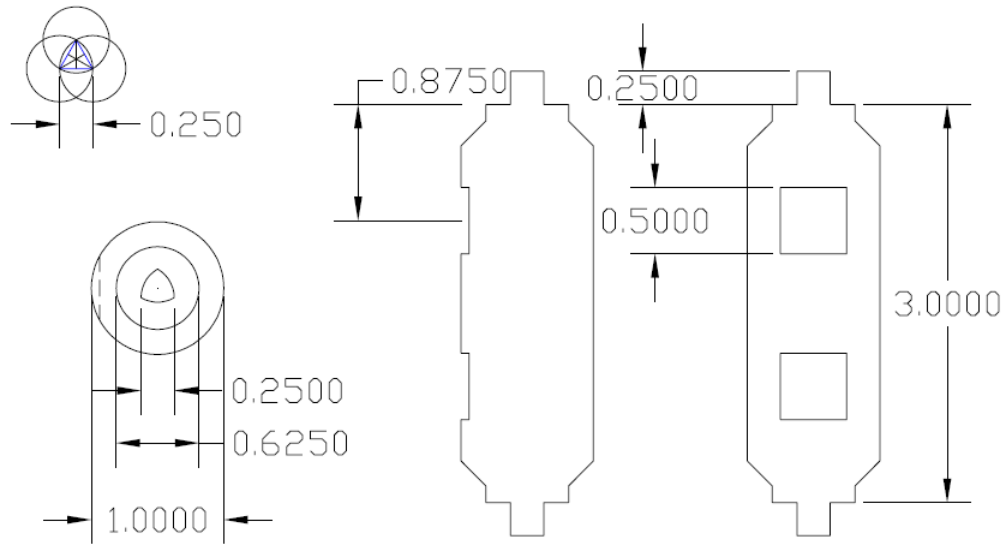


Figure 14 The Trivex Tool CAD Design. For welding the pin length was ground down to .237”

### 3.5 Position Control Welding Process

The motor drives mounted on the wall behind the FSW machine, along with the data from the various sensors and encoders, is all passed through a sensor box and to the control computer. Thus the tool position is known and controlled by a computer, all funneled to the user through a Graphic User Interface known as “Weld Controller” programmed by graduate student Paul Fleming. This program automates several of the sub-routines necessary for setting up and performing the weld, though these routines are called and directed by the user. A screenshot of the Weld Controller GUI can be seen in Figure 15.

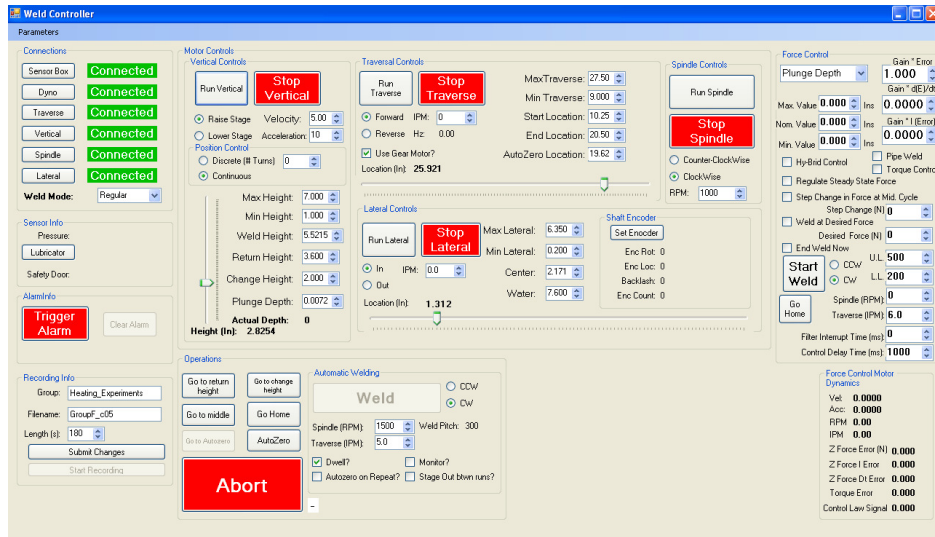


Figure 15 The Weld Controller Program GUI

The procedure for performing a heated weld using the Vanderbilt FSW machine and Weld Controller program is outlined below:

1. The thermocouples are loaded into the welding sample which is then mounted on the raised anvil with the clamping system.
2. The sensor box, motor drives, dynamometer, and thermocouple monitor program are turned on and connected in the Weld Controller program.
3. The vertical sensor is driven past its static zero reference mark.
4. The weld's parameters – start and end locations, plunge depth, spindle speed and direction, and the traverse rate – are input into the program.
5. The FSW tool is brought to the end of the weld sample and carefully aligned so that the back edge of the shoulder overlaps the sample while the pin misses.
6. The Autozero function in the Weld Controller is called. This process automatically brings the weld table up while monitoring the dynamometer for small changes in

force; once the tool shoulder makes contact with the weld sample the table height is recorded as the weld height.

7. By pressing “Go Home” on the program, the machine moves the tool to the front of the weld sample and raises the table to the weld height plus the plunge depth.
8. The thermocouple controller is turned on and the desired beginning weld temperature is set.
9. While the heating element, raised anvil, and weld sample heat up, the temperature is monitored both on the computer and on the thermocouple controller. The controller is adjusted as needed to bring the sample to the desired temperature.
10. Once the thermal conditions are right, nitrogen pressure is turned on, the thermocouple controller/heating element are turned off, and the “Weld” button is clicked on the Weld Controller program. The computer turns on the lubricator for 20 seconds before starting the spindle to ensure adequate oil in the spindle head. Once the spindle is started, the tool is slowly moved into the material, entering through the side. After an inch of moving slowly – creeping into the sample - the program pauses briefly and begins welding the sample in earnest at the settings entered earlier.
11. During the weld the force and torque readings of the Kistler dynamometer are recorded and stored in a text file. Separately, the position commands from Weld Controller are also recorded.
12. At the end of the weld sample the tool exits by traveling out of the far end. The tool is raised up above the clamping system and the spindle is shut off.

13. The clamps are removed, and the finished weld is labeled. The raised anvil, often hotter than the initial heating temperature due to the heat of the weld and the thermal insulation, is moved to another part of the machine table and allowed to cool before the next weld.

Based on previous welding done in the Vanderbilt welding lab with the Trivex pin design, all welds were carried out at 2000 rpm. Four traverse welding speeds were chosen for investigation: 5, 8, 11, and 14 ipm. The major independent variable, of course, was the initial temperature of each weld. Based off the work of Riichi et al. [15], after the room temperature control welds were finished, welds were completed with initial aluminum temperatures of 50, 75, 100, 150, 200, 250, and 300 °C. Because the autozero process was carried out before the heating, the plunge depth was decreased for the higher initial temperature welds to accommodate for thermal expansion: plunge depth was .0072” initially, .0064” for the 150 and 200 °C welds, and .0056” for the 250 and 300 °C welds. The weld matrix and naming convention is shown in Table 3.

Table 3. Position Control Weld Matrix. No shading indicates .0072” plunge depth, vertical shading is .0064”, and horizontal is .0056”

Traverse Speed (ipm)	Initial Welding Temperature (°C)								
	22	50	75	100	150	200	250	300	
5	A05	B05	C05	D05	E05	F05	G05	H05	
8	A08	B08	C08	D08	E08	F08	G08	H08	
11	A11	B11	C11	D11	E11	F11	G11	H11	
14	A14	B14	C14	D14	E14	F14	G14	H14	

### 3.6 Force Control Welding Process

Whereas most FSW done in the Vanderbilt lab is done using normal position control and records the forces, the Weld Controller program also contains the capability of FSW with force control instead. The programming and initial research for force control welding was done by graduate student Russell Longhurst. The two controllers are essentially the inverse of each other: while a position controller commands the movement of the tool, uses the position for feedback, and measures the process forces as the dependant variables; with force control a desired force level is the input, the process forces are the feedback, and one of the many weld parameters is the output and dependant variable.

For the force control welds, the Weld Controller monitored the axial force of the weld and controlled the traverse speed. The system was given an input desired axial force of 4000N based on the results of the previous position control welds. Each weld was also given an initial traverse speed also loosely based on the previous welding, though kept low to help prevent tool fracture at the start of the weld. During the weld a basic proportional controller scheme was used to achieve the desired axial force by adjusting the traverse speed: travel speed was increased to raise the axial force and slowed to reduce it. The overall traverse speed output was of course limited by the machine's capabilities. The C# source code for the traverse force controller is given in Appendix A; the characteristic equation for the controller is shown here as equation 1:

$$\Delta = ((1.0/2000.0 * ((F_{cn}Gain * Error) + (F_{cn}I_{Gain} * IError) + (F_{cn}DtGain * DError))))); \quad (1)$$

Delta is the adjustment applied to the traverse speed; Error is the difference between the measured and input axial forces, with IError the integral of that and DError the derivative

of that measurement. The integral and derivative gains (FcnIGain and FcnDtGain, respectively) were set to zero, and the proportional gain (FcnGain) was set to two based on previous work done with this force control model and the Trivex tool. This gave an overall proportional gain of 1 ipm change for every 1000 N of error.

The welding procedure for the force control welds was nearly identical to the one previously described. Obviously the input parameters changed as described; the only other difference was that around an inch from the end of the weld, the tool stopped traverse movement and the table dropped away, rather than having the tool exit out the end of the weld. The weld matrix, naming convention, and initial traverse speeds can be seen in Table 4.

Table 4. Force Control Weld Matrix

Initial Welding Temperature (°C)	Weld Name	Initial Traverse Speed (ipm)
22	Act	5
50	Bct	5
75	Cct	5.5
100	Dct	5.5
150	Ect	7
200	Fct	7
250	Gct	8
300	Hct	8

### 3.7 Post-weld analysis: Forces

Two comma-delimited data files are produced by the Weld Controller program for each weld. The first of these is the recording of the dynamometer data, including the measured X, Y, and Z forces, torque, and dynamometer position. Unfortunately, at 2000 rpm the ten-fin lower optical sensor is poling the dynamometer at 33.3 Hz, which is faster than the data acquisition system could run. As a result some data points were dropped; the system was switched to trigger with the upper optical sensor and ran without problems. The second data file of each weld is the recording of the weld parameters, machine commands, and tool position.

Matlab was used to analyze both data files for each weld. For the position control weld series, the axial force is of primary interest. Initial graphs of the axial force over the time of the weld showed noise, so the data was put through a moderate 9-point moving average filter to make comparisons easier. The average axial force for each weld was found from a 20 second window of the steady-state portion of the weld; 20 seconds was chosen as the fastest 14 ipm welds only include about 30 seconds of steady state data. Welding torque was calculated in the same way for each weld.

For the force control data there were two items of interest. Primarily the commanded traverse speed was investigated. This data was graphed over the course of the weld without any filtering. The average commanded weld was computed from the last half of each weld to ensure the controller had enough time to settle into a steady state. The second measurement of interest is the axial force error: the difference between the desired and recorded axial forces through the weld. This measurement is used primarily to evaluate how well the controller equation is working.



### 3.8 Post-weld Analysis: Metallography

To investigate the microstructural cross-section of a weld, the sample must first be prepared properly. The first step is to cut a small cross-section out of the middle of the weld; the spot is carefully chosen to make sure the cross-section is from the steady-state portion of the weld. A diamond saw is used to cut the face of the cross-section to ensure a smooth surface. The cross-section face is then polished using a polishing wheel with successively finer grades of Silicon Carbide paper: beginning with 300 grit and graduating to 600, 800, 1200, 1600, and finally 2400 grit paper. At this point the cross-section surface is mirror-like without any scratches or abrasions. To help really bring out the microstructure features the sample is etched by covering with Keller's reagent, a solution of 5% Nitric acid, 5% Hydrochloric acid, 5% Hydrofluoric acid, and 85% Water. After etching an optical microscope and computer were used to capture the macrograph images as well as investigate the grain structure of the weld.

## CHAPTER IV

### RESULTS

#### 4.1 Position Control Weld Results

Figure 16 is a graph showing the typical shape of the axial force vs. time graphs generated for each of the position control welds. This particular graph is for weld E11. The initial creep-in can be seen in the lower plateau of the axial force from 20 to 35 seconds into the weld; the program pauses briefly an inch into the material (from 35 to 39 seconds in) and then welds in earnest, seen as the large plateau beginning approximately 40 seconds into the weld. The end effects of the weld sample can also be seen by the steep fall off in axial force at the end of the weld; of course the axial force drops sharply once the tool leaves the aluminum.

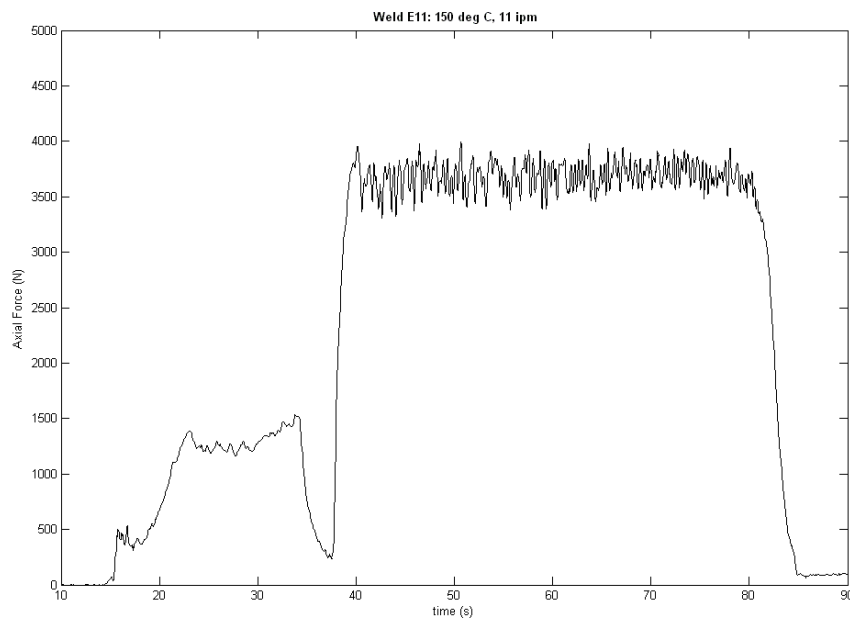


Figure 16 Weld E11, Axial Force (N) vs. Time (s)

The actual welding portion of all 32 axial force graphs can be seen in Appendix B. Some of these plots show a distinct rising trend in the force as the weld went along. In all of these the axial force rose evenly through the weld and exhibited a gain of between 150 and 300 N between the beginning and end of the weld. Figure 17 shows an example of this trend, focused in on the time of the actual welding. It is believed this trend is caused by the raised anvil sitting unevenly; most likely the small K-type thermocouple inserted between the heating element and the steel caused the finishing end of the anvil to sit high. Overall 12 of the 32 position control welds showed this rising trend in the axial force data; because the average force data was computed from the earlier portions of the weld, this small upward trend in some of the welds does not significantly affect the overall data.

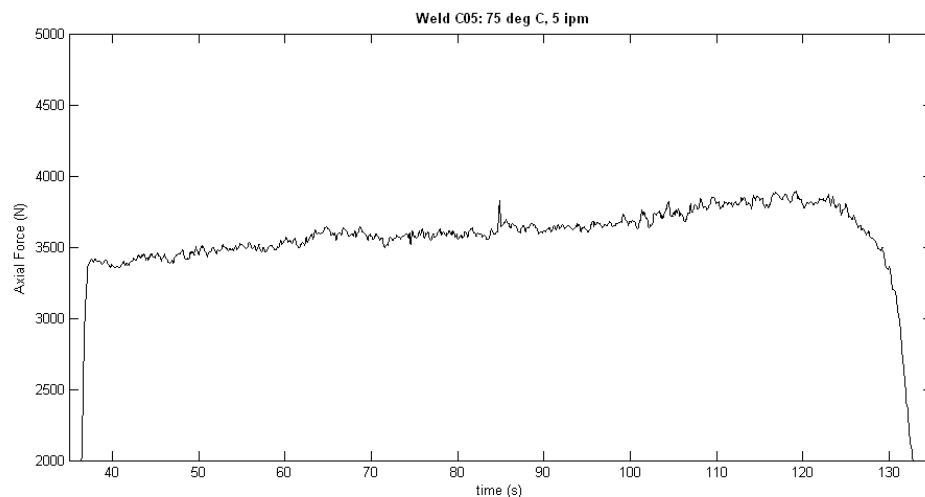


Figure 17 The Rising Trend in the Axial Force Graph for Weld C05

Comparing the axial force of multiple welds on the same graph is made difficult by the noise in the graphs as well as the sheer number of them. Even split up by traverse speed there are still eight initial temperatures to compare, so the average force graphs become much more practical. Specifically, comparing the average axial force for each

weld allows us to see trends in that force as the initial material temperature goes up. The average axial force for each weld is presented in Figure 18 and clearly shows an overall decreasing trend for all four travel speeds. Each curve definitely has a higher-order polynomial curve to it, with the axial forces rising after a local minimum and then falling off again at the highest initial temperatures. To better see the effect of the heating, the average axial force of each weld was normalized to the control weld (room temperature) for that travel speed; this normalized graph is seen in Figure 19.

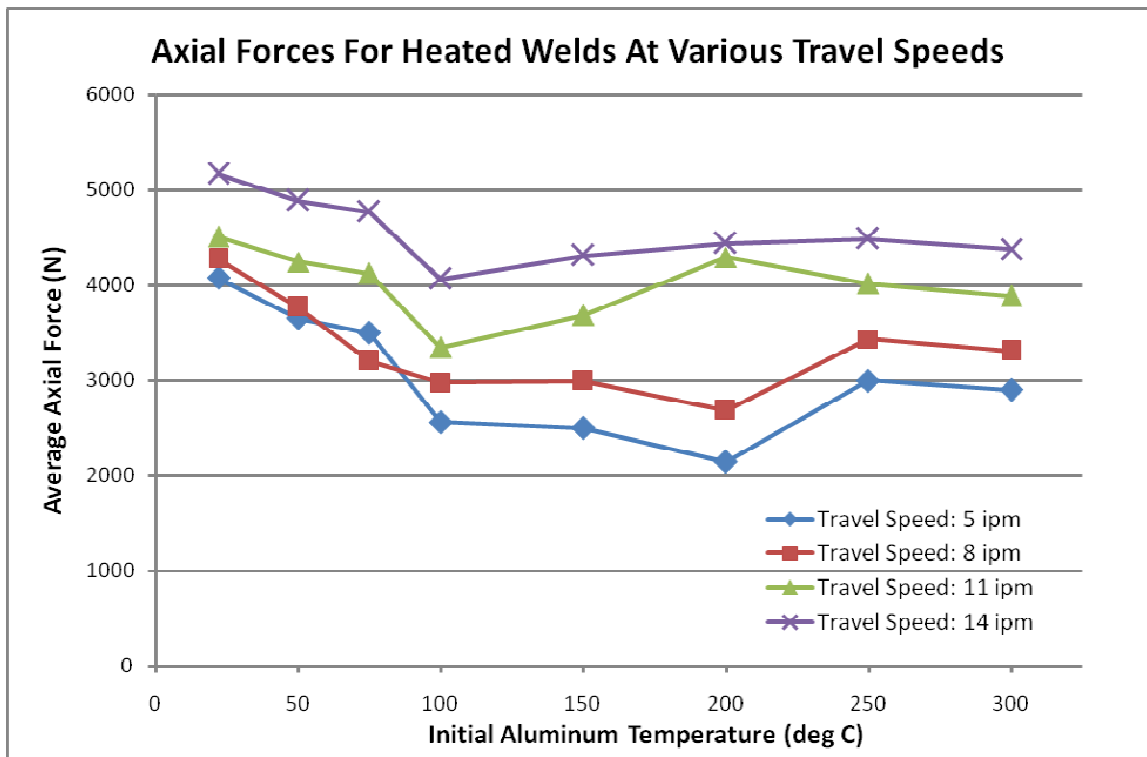


Figure 18 Average Axial Forces for the Position Control Welds

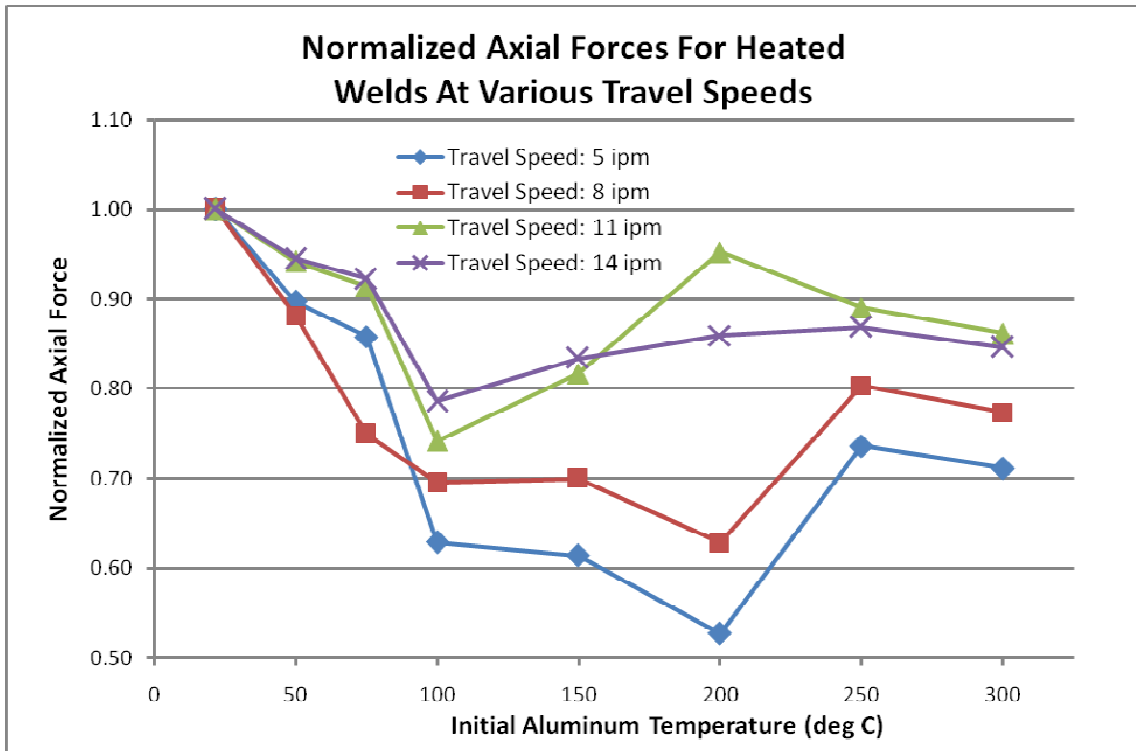


Figure 19 Normalized Axial Forces for the Position Control Welds

The average torque was also computed for each of the position control welds. The torque values are most useful as an easy way to calculate the power consumed in the FSW: power is simply torque multiplied by the frequency of the weld. Since all welds were performed at 2000 rpm, or 33.33 Hz, the power figures are exactly proportional to the torque values. Both average torque and average power for these welds are graphed in Figure 20, and the normalized values presented in Figure 21. Unlike the axial force graphs, the decreasing trend in the torque graphs seem to be much closer to linear, though at the higher temperatures they appear to begin converging.

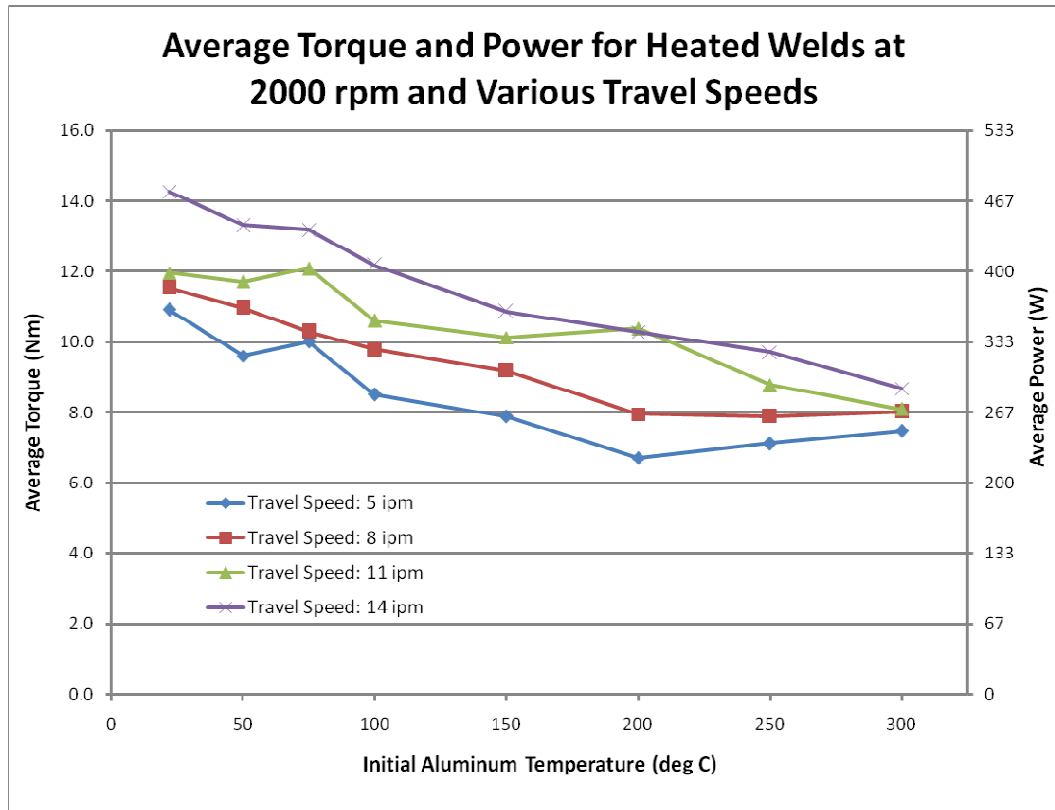


Figure 20 Average Torque and Power Values for the Position Control Welds

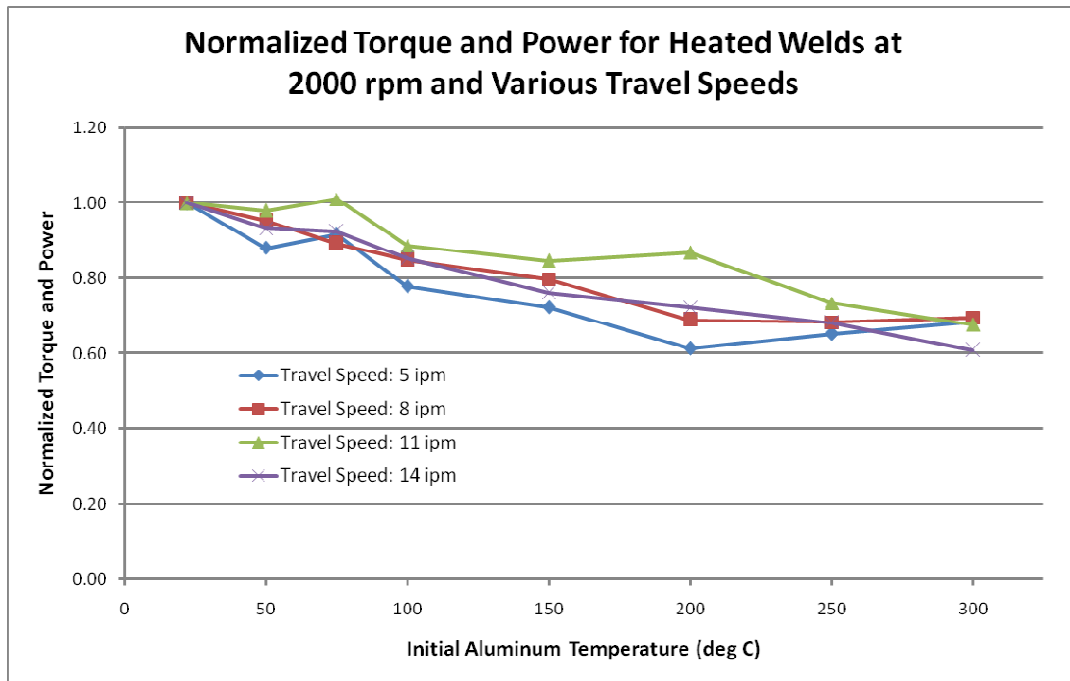


Figure 21 Normalized Axial Forces for Heated Welds at Various Travel Speeds

The cross sections for the position control welds were remarkably consistent. A wormhole weld defect was found in nearly every weld on the lower advancing side of the nugget. The size of the wormhole varied with the initial temperature of the weld; the progression can be easily seen in Figure 22, which shows the macrographs of all eight 11 ipm welds. The hole in the bottom of weld H11 was created when removing the weld from the anvil, as the welding forces had partially joined the aluminum to the steel. In about half the welds there was a surface lack of fill defect, seen on the top of the weld also on the advancing side: in Figure 22, welds B11, C11, and D11 all show this. In some welds it is observed that the two defects seem to be related – the worm hole defect travels up to the surface hole – indicating a lack of flow along the entire AS of the weld nugget. This is seen in weld C14, shown in Figure 23.

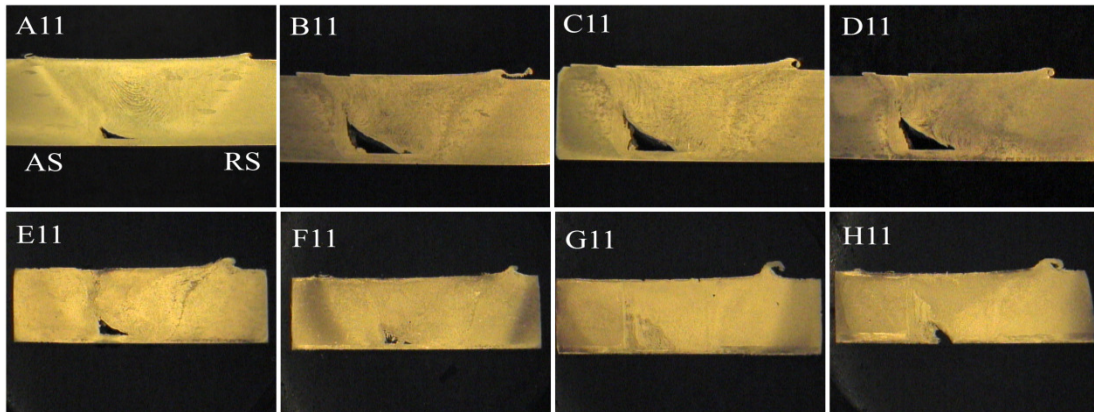


Figure 22 Macrosections of the 11 ipm Welds

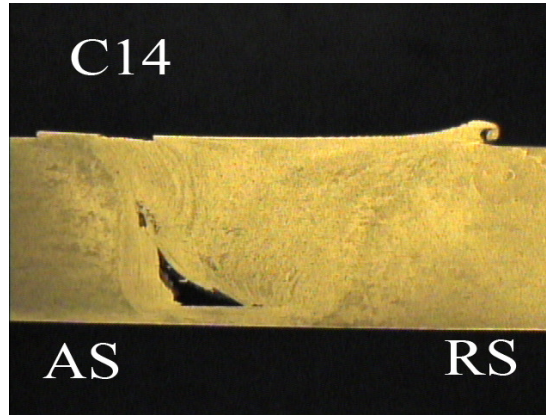
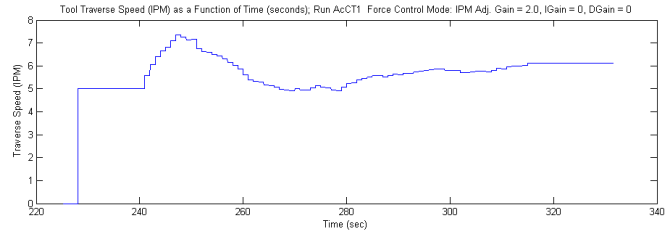
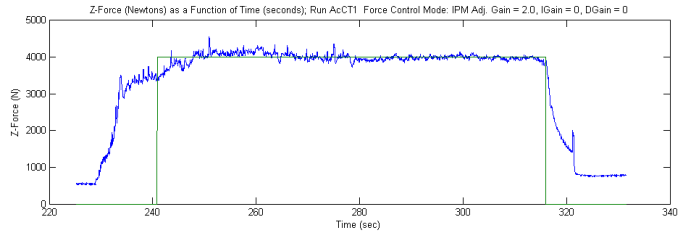


Figure 23 The Connection Between the Two Defects

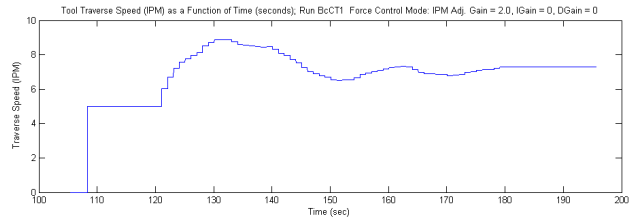
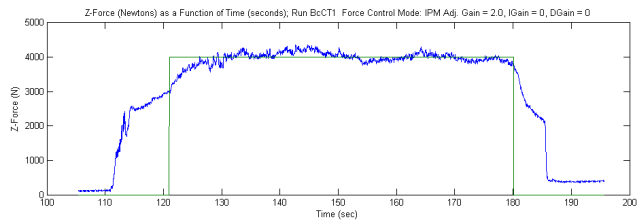
#### 4.2 Force Control Weld Results

As discussed before, there were two graphs of interest for each weld performed with the traverse force control method. The first of these generated in Matlab is the comparison of the actual axial force during the weld with the commanded 4000 N level. The command signal in these graphs also marks when the force control is turned on and off, as the beginning of the weld is less clear than in the position control welds. The second graph created for each weld shows the commanded traverse speed, which is the output of the controller and primary dependant variable. These two graphs are shown for each force control weld performed in Figure 24. The results show that the basic proportional controller equation is working very well; in the last half of each weld, as the steady state was reached, the errors were generally less than  $\pm 100$  N. Welds Gct and Hct show the most error at around  $\pm 300$  N.

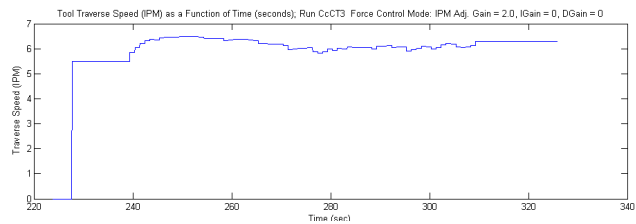
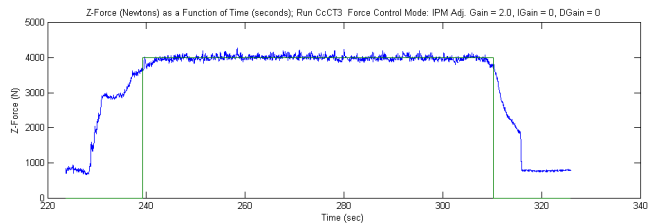




(A) Weld Act, no heating

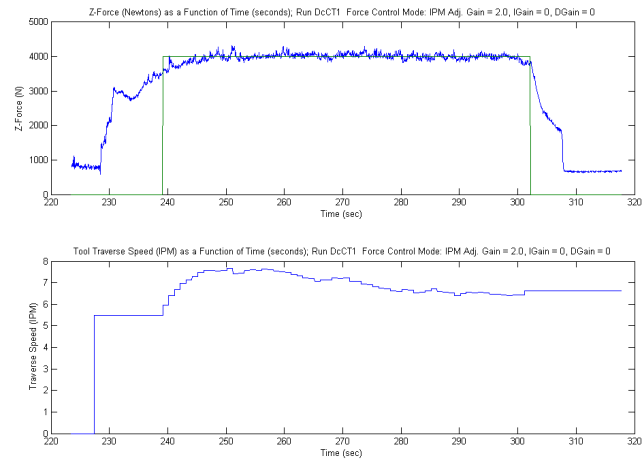


(B) Weld Bct, 50 °C Initial Aluminum Temperature

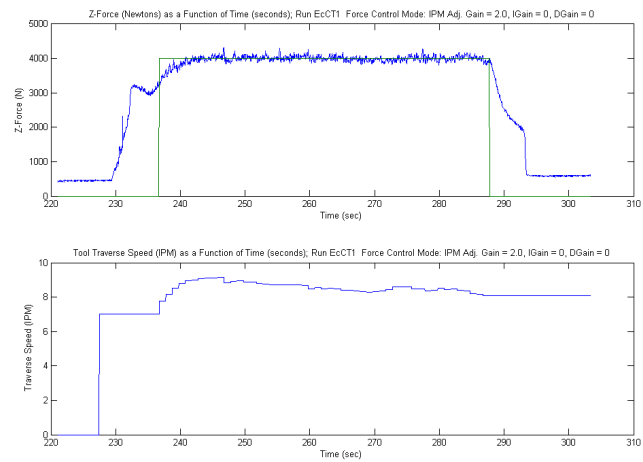


(C) Weld Cct, 75 °C Initial Aluminum Temperature

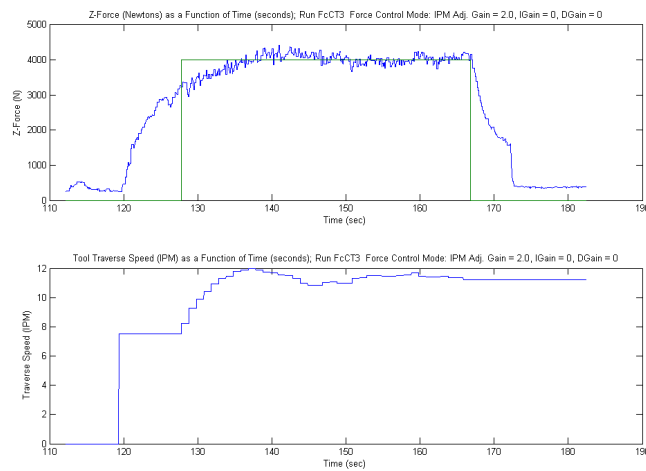
Figure 24 Individual Force Control Weld Graphs



(D) Weld Dct, 100 °C Initial Aluminum Temperature

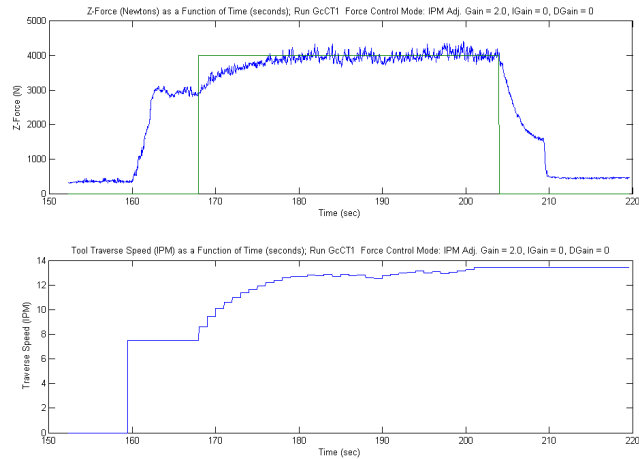


(E) Weld Ect, 150 °C Initial Aluminum Temperature

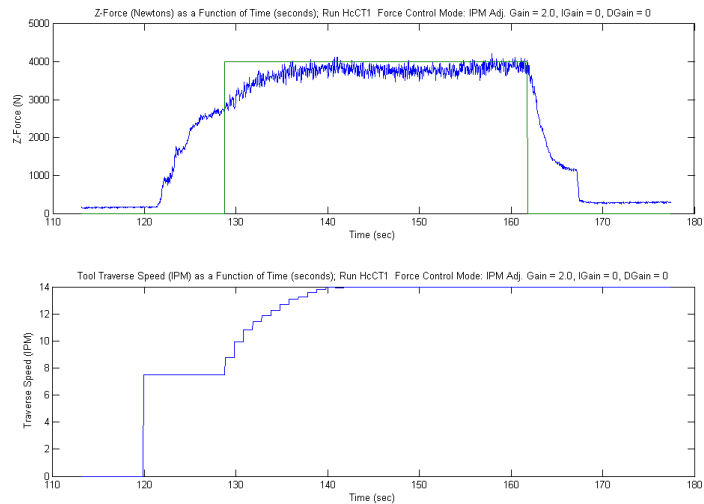


(F) Weld Fct, 200 °C Initial Aluminum Temperature

Figure 24 Continued



(G) Weld Gct, 250 °C Initial Aluminum Temperature



(H) Weld Hct, 300 °C Initial Aluminum Temperature

Figure 24 Continued

To look at the overall picture the average command traverse speed was computed. Given that the beginning traverse speeds were guesses, and low guesses at that to prevent tool damage, the average speed values were computed from the last half of each weld. These average values, plotted against the controlled initial aluminum temperature, are given in Figure 25.

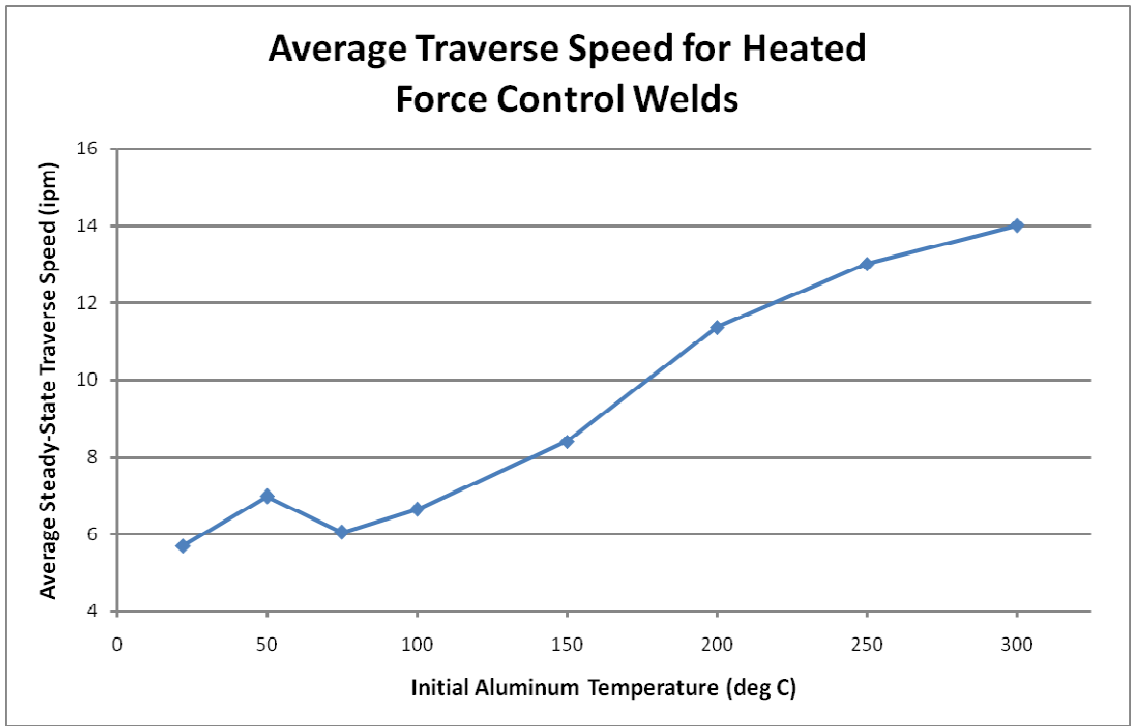


Figure 25 Average Force Control Weld Results

## CHAPTER V

### DISUCSSION

#### 5.1 The Reduction in Axial Forces

Overall the heating of the aluminum with an additional source beyond the FSW tool has definitely reduced the major process force associated with this new type of welding. As shown in Figure 19, with even small amounts of heating, the average axial force of welding AA6061 at some temperature dropped by a minimum of 21% for all welding traverse speeds. The maximum reduction seen was a great 43% reduction in force for weld F05 compared to the A05 control weld. These magnitudes are in agreement with the limited data found in literature [11].

Thinking about the average force data another way, by adding even slight preheating capabilities the travel speed or tool life of FSW can be significantly improved. If a tool was shown to have good wear characteristics under a certain load, the allowable travel speed could be easily doubled or almost tripled with additional energy input. Looking at Figure 18, weld A05 was performed without heating, 5ipm, and developed an average axial force of just over 4000 N. Weld D14 also developed just over 4000N of axial force, traveling at nearly three times the traverse speed, and the only difference was that the aluminum was heated to 100 °C before welding.

The force-control welds support this last point in the strongest possible way. Given a constant force input, Figure 25 demonstrates how much faster the system can travel for a given initial material temperature. The final data point on the graph should be

a bit higher in fact – that is, the traveling faster – but the force controller equation hit upon the 14 ipm traverse limit. We can see in the top graph of Figure 24 (E) that the recorded axial force never truly reached the 4000 N goal, meaning that characteristic controller equation would still be working to increase the travel speed even as the machine’s capabilities were maxed out.

Certainly the most intriguing result from the position control welds is the definite trend exhibited by all four traverse speed weld series in Figure 18. In each group, as the initial aluminum temperature increases, the average axial force decreases. This behavior was expected given aluminum’s yield strengths’ dependence on temperature, as shown back in table 1. Between 100 and 250 degrees Celsius pre-heating, however, each traverse speed trend actually increases, passing through an inflection point at around 150 degrees. After reaching a local maximum axial force at 200 or 250 degrees, each trend line finally drops off again at the highest temperatures. The characteristics of the trend definitely seem to be influenced by the travel speed. As the travel speed increases, the location of the local minimum moves to lower temperatures, and the latter half of the curves are broader than welds performed at slower traverse speeds.

## 5.2 Discussion of the Average Welding Torque

The torque curves present another interesting dimension of the heated welds. On the surface, the graphs are simple and make sense: as the material’s initial temperature is increased, the amount of force required to weld it – and thus the power needed for the FSW process – goes down. However, the hotter ends of the welds, especially the lower traverse speed welds, indicates something interesting happening. In Figure 20, for the 8

ipm welds the decreasing torque curve seems to flatten out and settle on 8 N-m for the three hottest welds. The 5 ipm trend dips below this value but actually rises up for these three hottest welds, also approaching 8 N-m of average torque.

As discussed in the introduction, the FSW tool performs two major functions: it heats the weld through friction and then stirs the material together. The process is essentially self-regulating: as the weld environment heats up the frictional load decreases and so does the heat input. When the material being welded is already heated, this regulating nature means that not only will the tool's overall load drop, as shown by the decreasing forces, but the load experienced by the tool is proportionally more to stir the material and less to create frictional heating. The slight convergence seen in the average torque values at higher initial temperatures could show how much power is required to simply stir the aluminum, as the frictional loads are entirely gone.

### 5.3 Fixing the Weld Defects

The large worm holes present in nearly all of the welds, along with the surface lack of fill defects, are a somewhat expected result given the use of the Trivex welding tool. While the tool design does provide more stirring action than a basic cylindrical pin it still lacks any of the surface features well known for creating lots of material flow. Kumar and Kailas discuss the presence of two primary flows in FSW: the first is a vertical pin-driven flow and the second a rotational shoulder-driven movement [17]. The worm holes in the bottom corner of the nugget suggest that the pin is not moving enough material vertically. Further, the shoulder is letting material escape the tool before it can bring it around behind the pin; close examination of Figure 22 shows this small amount

of flash on the surface RS of each weld. In the more extreme cases the shoulder loses enough material that a hole forms on the top of the AS of the weld.

The heating of the aluminum definitely played a part in helping solve these defects. With the material already warm, the FSW tool is logically able to create more stirring. However, the defects in this particular experiment are believed to be effectively eliminated with the use of a different tool design. A simple inclusion of threads – a common FSW tool feature – would create a vastly improved pin flow. A slightly larger shoulder would also help prevent material from leaving on the RS, thus helping solve the surface defect and feeding more material into the pin flow. This improved tool would create good quality welds while still experiencing the reduction in process forces that heating can provide.

#### 5.4 FLUENT CFD Modeling of Heated FSW with a Trivex Tool

To help explore the process forces and flows of heated FSW, the finite volume CFD solver Ansys FLUENT was used with implicit formulation to create a model of the welding process. The model was constructed by Vanderbilt graduate students David Lammlein and Chase Cox. The weld material viscosity function was set to Carreau model viscosity with a time constant  $\lambda = 10$  seconds, power-law index  $n=0.2$ , reference temperature  $\alpha=300$ , zero-shear viscosity  $1e8$  kg/m/s, and infinite shear viscosity of  $0.001003$  kg/m/s.



The total heat input was calculated via the weld power method [18-26]:

$$P = \omega \cdot M \quad (2)$$

$$Q = P \cdot \eta_{\text{thermal}} \cdot \eta_{\text{conduction}} \quad (3)$$

where  $P$  is the weld power (W),  $Q$  is the heat input to the tool and weld material (W),  $\omega$  is the tool rotational speed (rad/s),  $M$  is the measured torque (N·m),  $\eta_{\text{thermal}}$  is the fraction of mechanical work dissipated as heat into the tool shank and the weld, and  $\eta_{\text{conduction}}$  is the fraction of that heat input into the weld. Values of 0.90 and 0.75 are used respectively for these terms and are found to be reasonable for the conditions of the current study. The measured torque values came from the 5 ipm weld series in Figure 20. This calculated total heat input was then applied in the model at the tool-material interface via a user-defined function which varies heat input over the tool surface according to the local tangential velocity magnitude. Heat input is therefore highest near the tool shoulder edge and zero at the center of the probe tip with the total heat input equal to the weld power. A variable slip shear condition was set at the weld interface. The tool rotational velocity was set to 72% of the experimental parameter and a pure stick condition was used. This simple boundary condition was used because the actual relationship is unknown and unwarranted complexity is not desired in the model.

The CFD model consists of 171395 tetrahedral elements which accurately reflect the experimental geometry. The tool traverse was imposed in the model by leaving the tool at the model origin and establishing a velocity inlet and pressure outlet for the aluminum plate. Element refinement was increased towards the weld interface; the surface elements of the tool pin are seen in Figure 26. The thermal boundary conditions used in the model are shown in Figure 27.

Due to the high tool rotational velocity, large heat input, and high viscosity of the experimental situation, relatively steep gradients in pressure and temperature exist in the Fluent model, particularly near the tool surface. These conditions mean that this case and FSW in general are on the edge of what Fluent software can handle. Certain techniques were therefore employed to arrive at a valid solution, which converged in all variables. These techniques were first a lowering of the under-relaxation factors to 60% of their default values and second a gradual adjustment of viscosity and tool angular velocity with intermediate iterations.

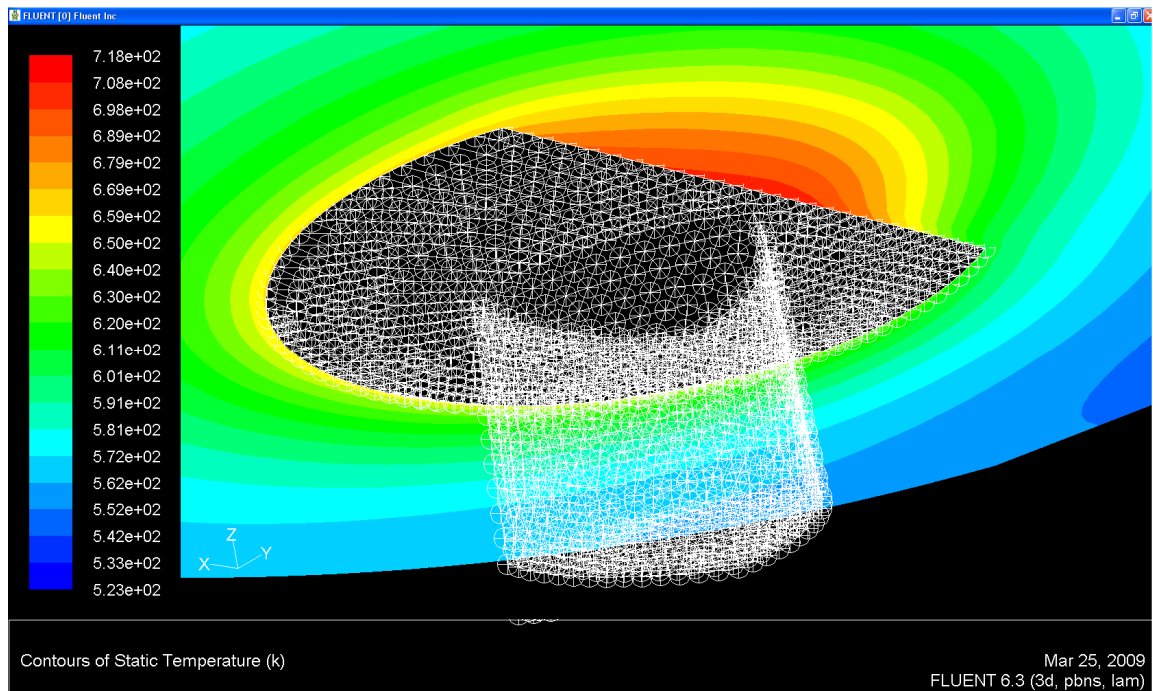


Figure 26 Detail of the Trivex Pin Model Elements

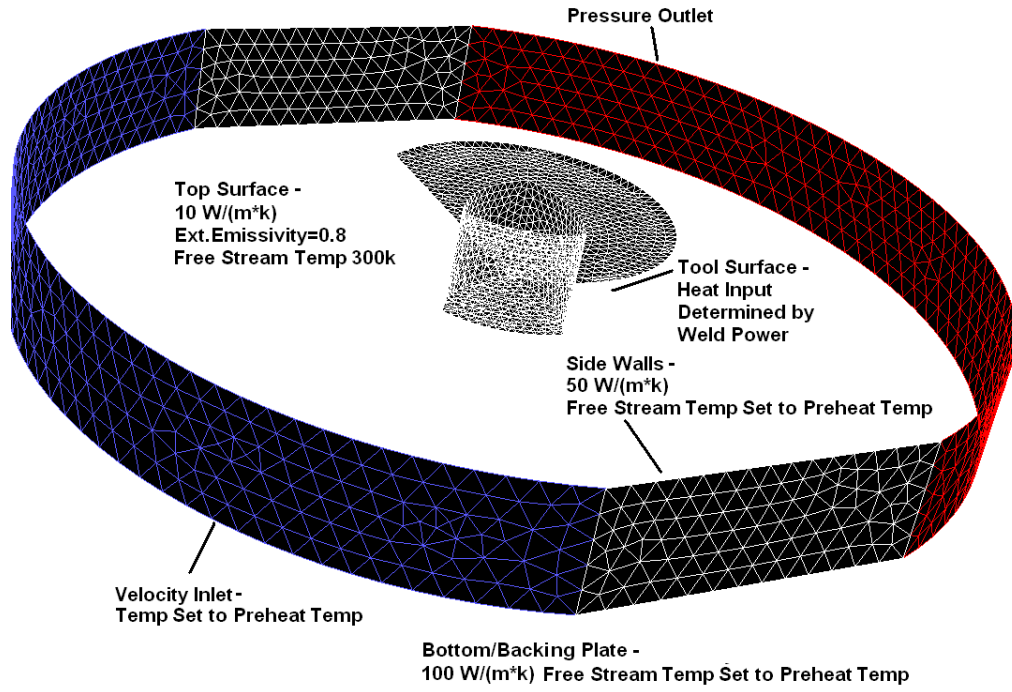


Figure 27 FLUENT Model Thermal Boundary Conditions

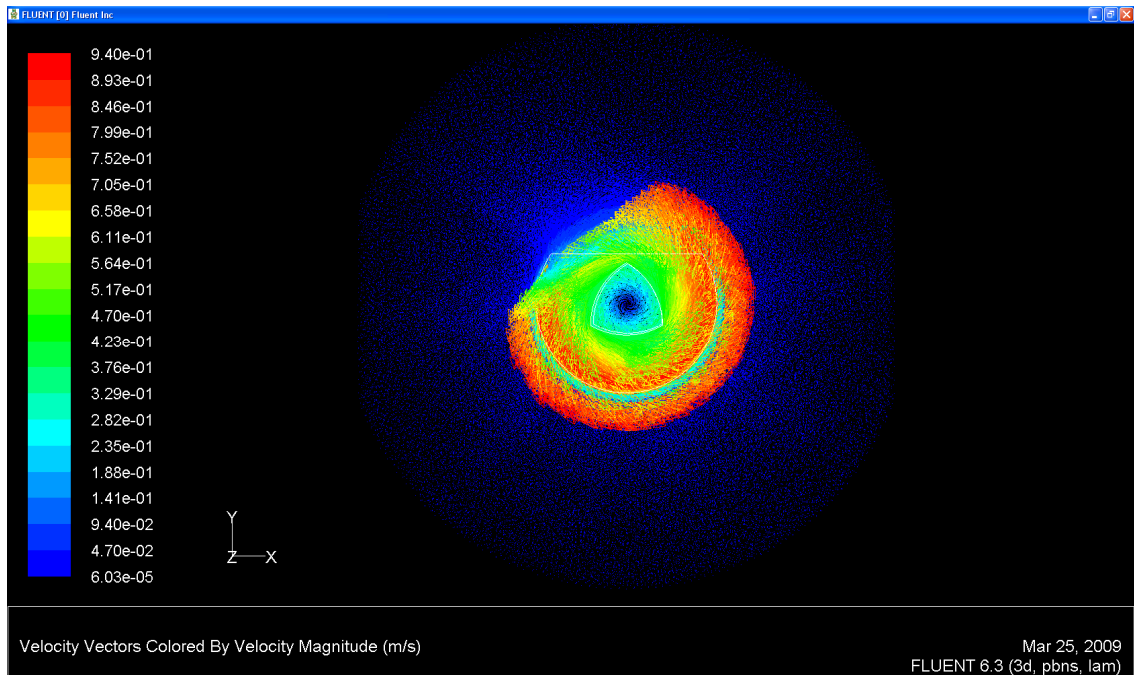


Figure 28 FLUENT Material Flow Vectors

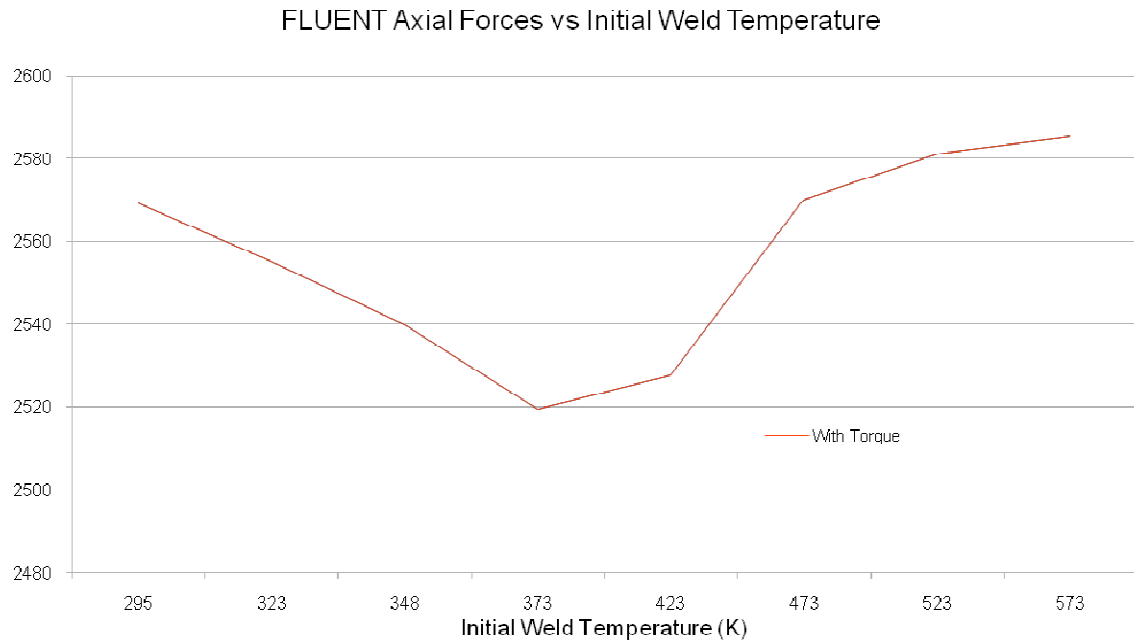


Figure 29 FLUENT’s Axial Forces for Varying Initial Weld Temperatures

The FLUENT model captures many of the interesting features of the welding experiments. Figure 28 is a top down view of the material flow around the tool. The disruption of the shoulder flow is easily seen. A similar lack of flow around the pin is present in the same area, though the top down view makes this harder to see. Obviously this flow data corresponds with the defects seen in the experimental weld macrographs.

More exciting, the same general trend seen in the average axial force data for the position control welds is seen to a small extent in the force data from the CFD model. This definitely helps confirm a few things about the experimental results. First, the FLUENT results support that the trends seen in Figure 18 are real. Further and more importantly the modeling results suggest that the axial force curves are created by the process of FSW in aluminum 6061-T6, and not artifacts created by the elaborate insulated, raised-anvil setup built to heat the welds in the first place.

The FLUENT results also help to understand the mechanism behind the fluctuating average force values. One plausible explanation was that the heating period before the weld began was acting to heat treat the aluminum weld samples. Even with the fast powerful mica heating element, the higher initial temperature welds took some minutes to reach those initial temperature – as long as 15 minutes for the hottest welds – and it was speculated that the time allowed some type of precipitation hardening to begin, strengthening the aluminum above expected values. However, the CFD model does not contain this heating time and yet exhibits the same basic force trend; we must conclude that the axial force fluctuation over initial temperature comes from material properties and FSW mechanics themselves.

### 5.5 Conclusions and Future Work

While “preheating” or “assisted” FSW has been suggested and performed by many, this is one of the first studies to take a measured and controlled look at how that heating affects the process forces of this relatively new joining technique. Already here at Vanderbilt another graduate student is using the heating set-up to help his attempts to reduce forces and increase stirring while joining dissimilar materials. As seems usual in FSW, the experimental work into preheating has outpaced the technical understanding of the process. Hopefully this experiment, while still an experimental approach, can help prompt more controlled examinations and a better understanding of the preheating process.

There are obviously plenty of applications out there for assisted-FSW as the growing industry looks to weld harder materials with less forces and tool wear. On the

more theoretical front examining heated FSW with another material – either another aluminum alloy or something entirely different – would provide great insight into the nature governing the force reduction trends seen in this document. Performing mechanical testing on the finished welds, along with pieces of the parent material not welded, would help definitively prove whether or not any type of additional heat treating was occurring. Another advance would be to recreate this work with other tool designs to prove that additional mechanical stirring can produce sound, defect-free welds without losing the significant advances from heating.

## Appendix A

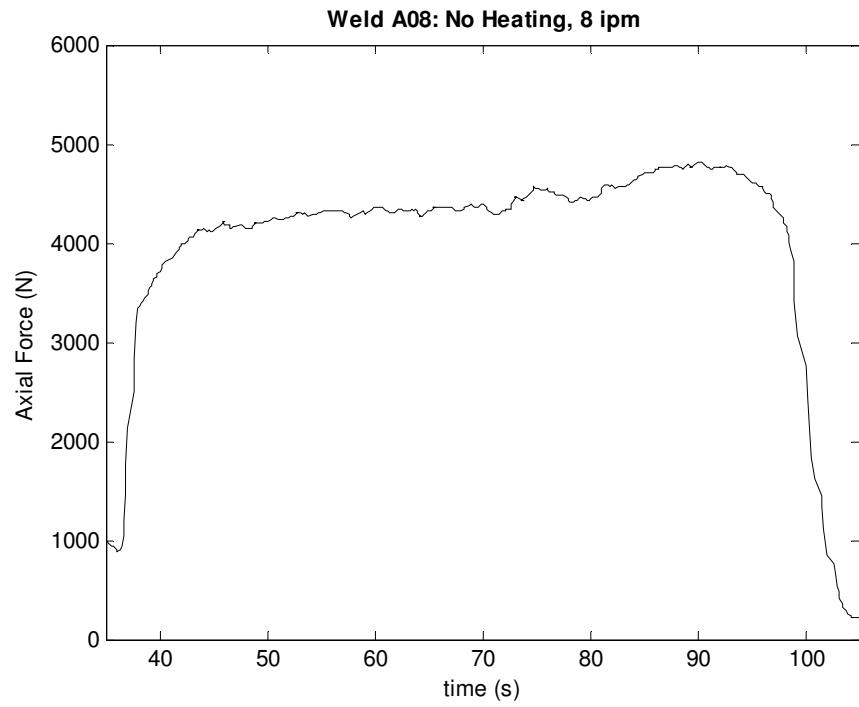
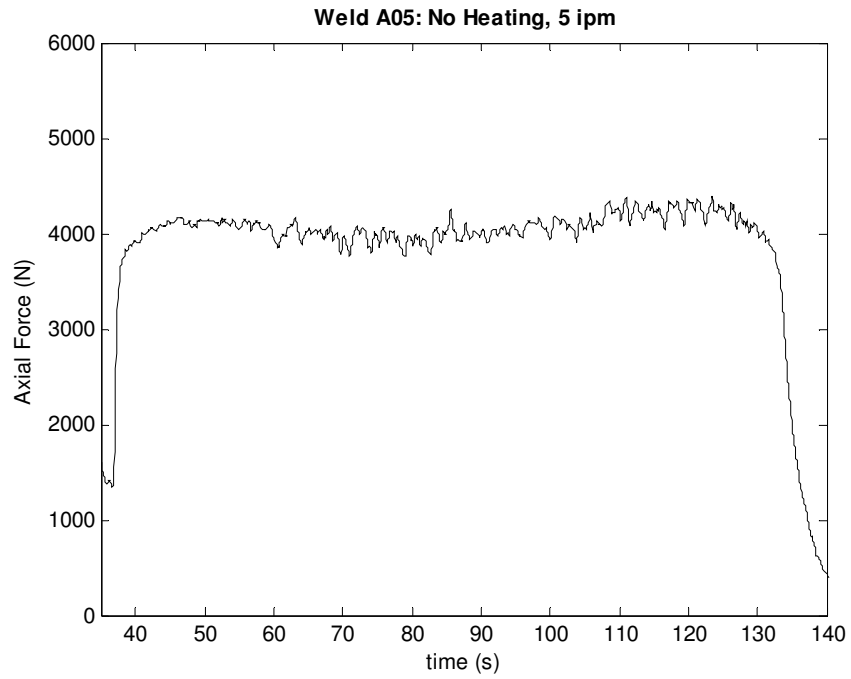
### Source Code for the Traverse Speed Force Control Programming

```
else if (FcnMode == 2) //Adjust Force by changing Traverse Speed.
    //Increase IPM to increase Z Force. Decrease IPM to decrease Z Force.
{
    if (Math.Abs(Error) > 0) // Adjust IPM if Force Error is outside the Deadband Zone of 0 N.
    {
        //Control Law = (1 IPM per 2000 Newtons) x PID
        Delta = ((1.0 / 2000.0 * (((FcnGain * Error) + (FcnIGain * IError) + (FcnDtGain * DError)))));
        //Check to see if new IPM would be within the tolerance.
        if (((Delta + IPM) > FcnMinVal) && ((Delta + IPM) < FcnMaxVal))
        {
            // Increase or Decrease IPM to new value.
            ChangeTraRef((double)(Delta + IPM));
            // Record new IPM value.
            IPM = ((double)(Delta + IPM));
            Thread.Sleep(delay);
        }
        else if ((Delta + IPM) > FcnMaxVal) //if new IPM is above the tolerance....
        {
            ChangeTraRef((double)(FcnMaxVal));
            IPM = ((double)(FcnMaxVal));
            Thread.Sleep(delay);
        }
        else if ((Delta + IPM) < FcnMinVal) //if new IPM is below the tolerance...
        {
            ChangeTraRef((double)(FcnMinVal));
            IPM = ((double)(FcnMinVal));
            Thread.Sleep(delay);
        }
    }

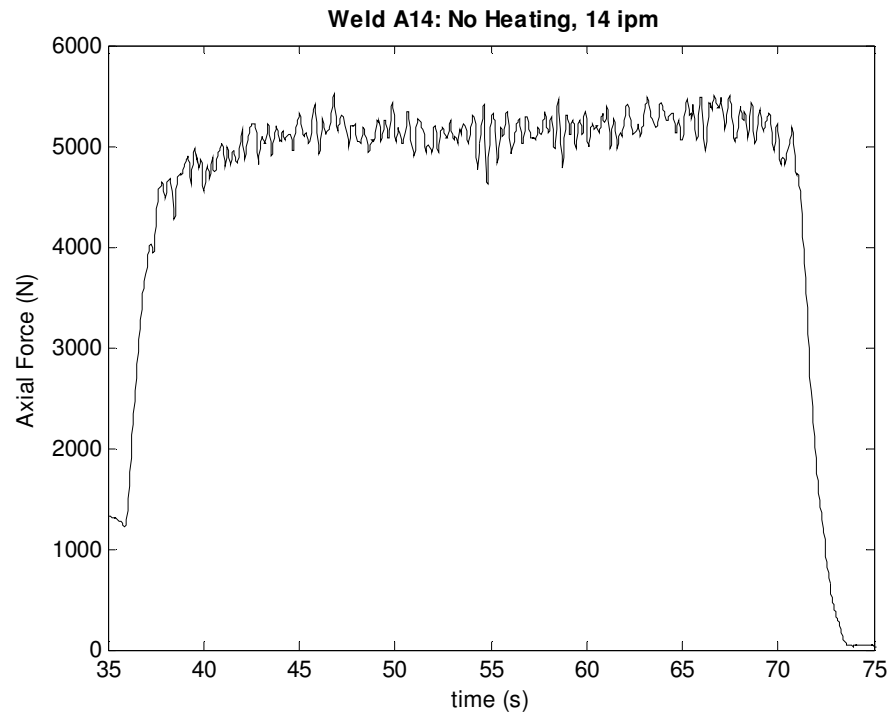
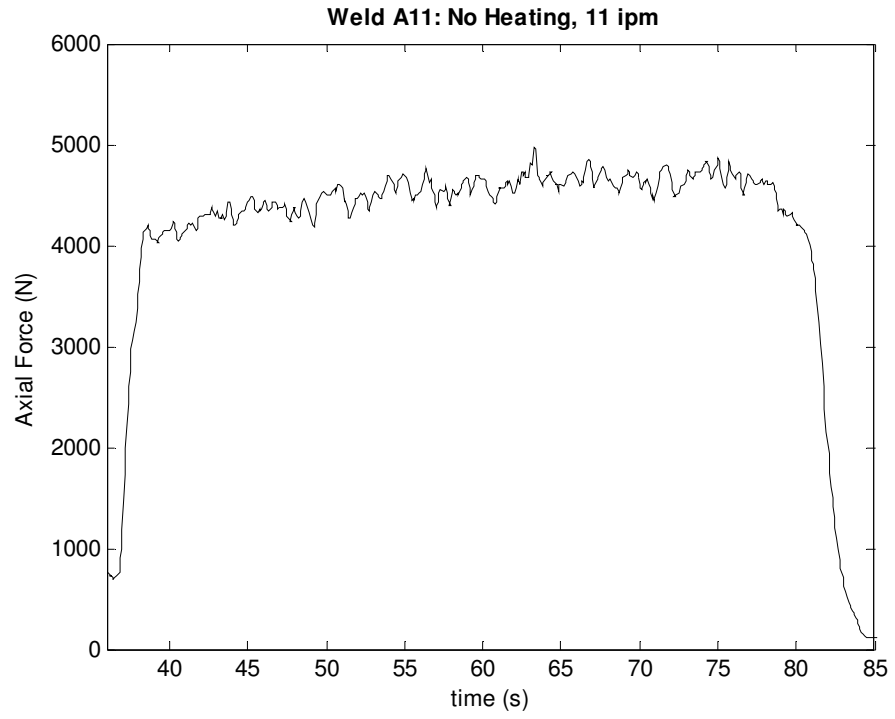
    //Do Nothing. Z Force is withing 0 Newtons of the desired force.
    else if (Math.Abs(Error) < 0)
    Thread.Sleep(delay);
}
```

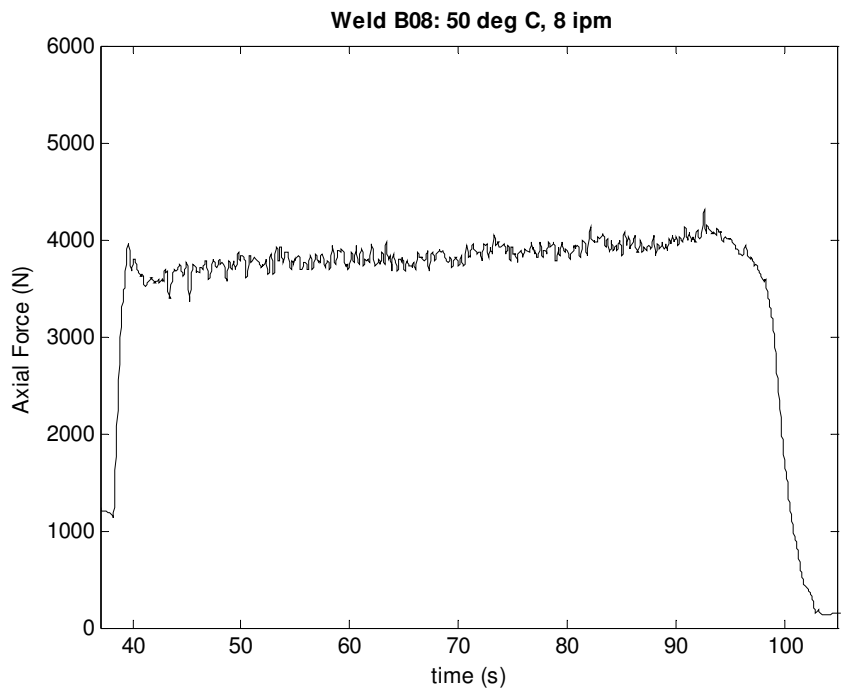
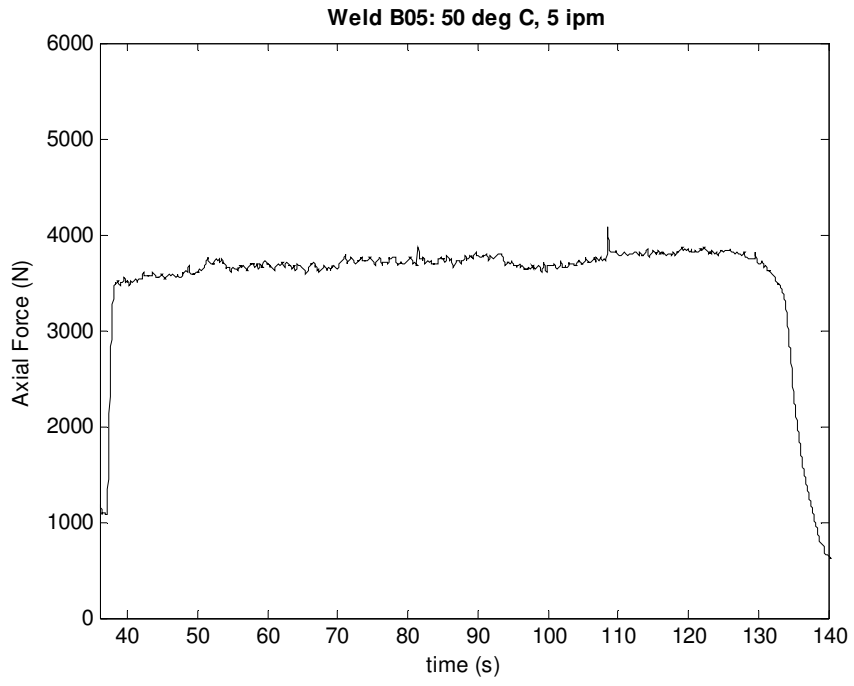
## Appendix B

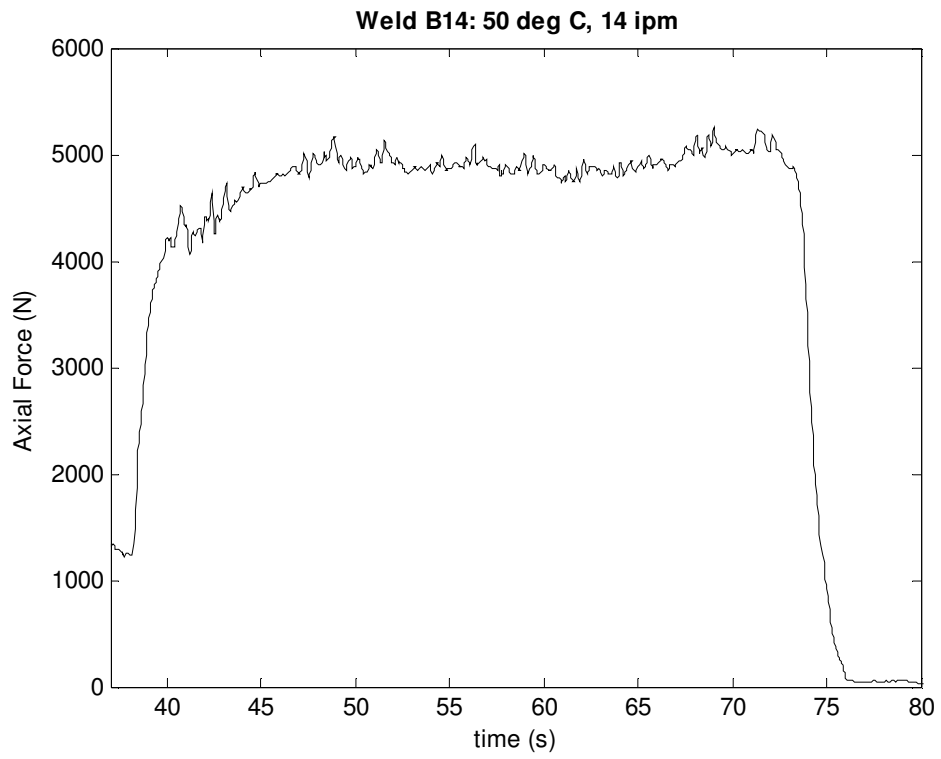
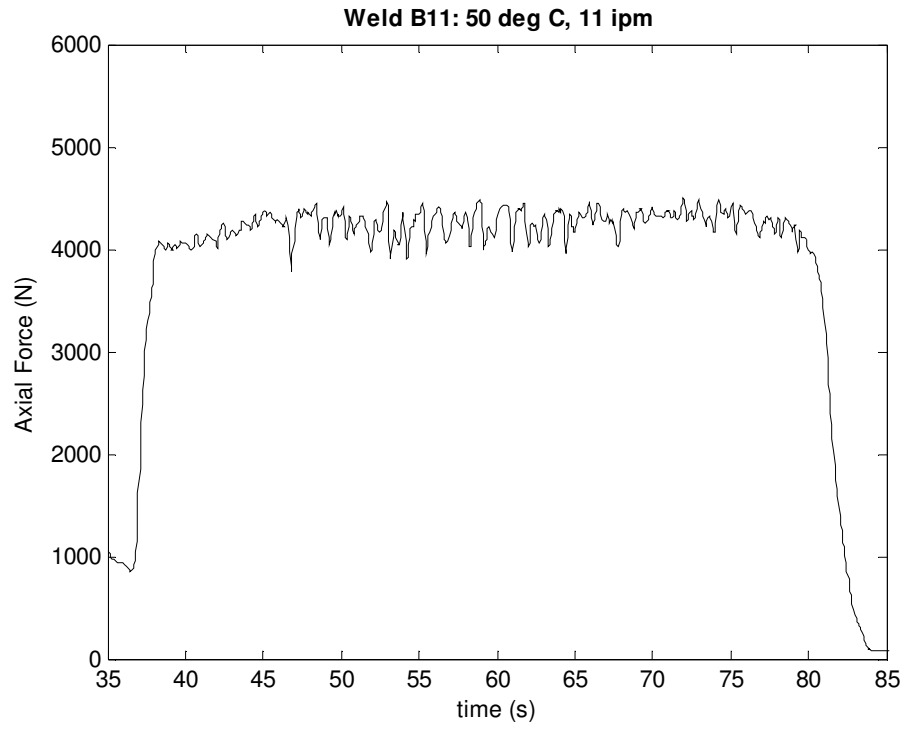
### Position Control Weld Axial Force Plots

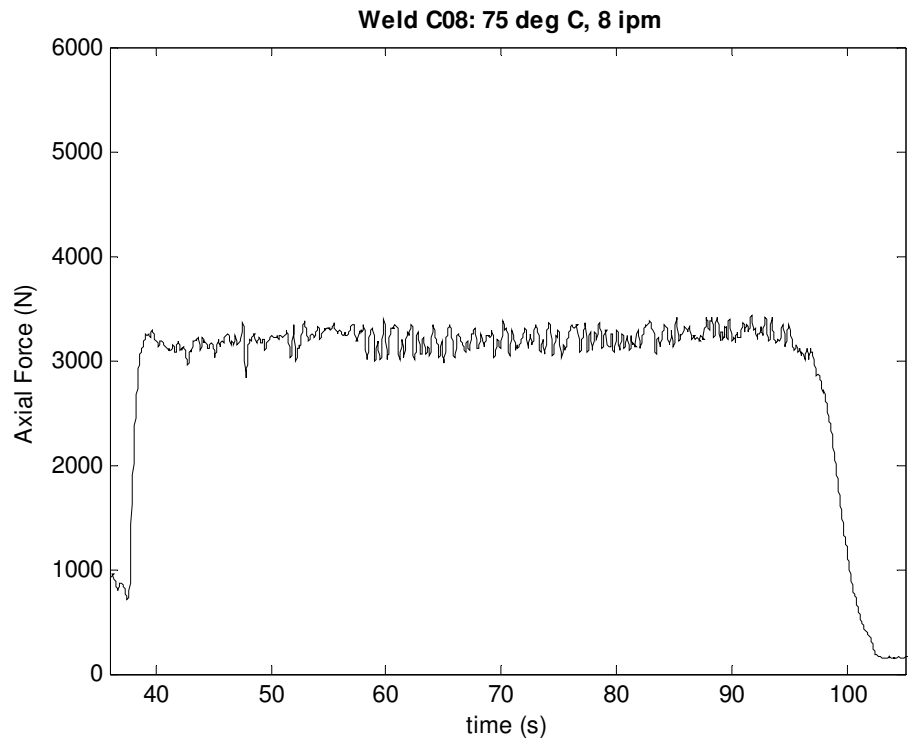
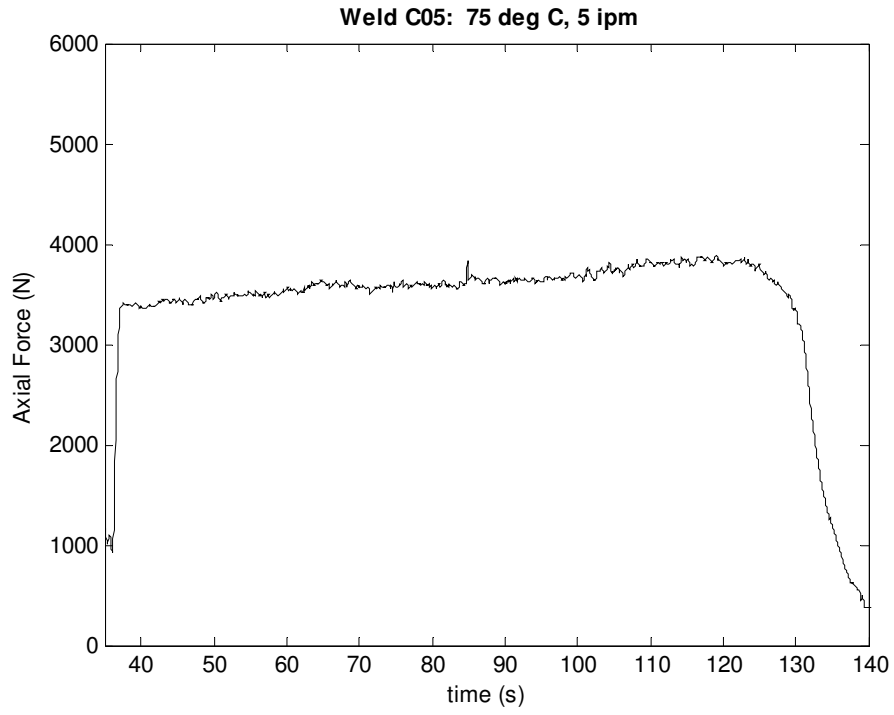


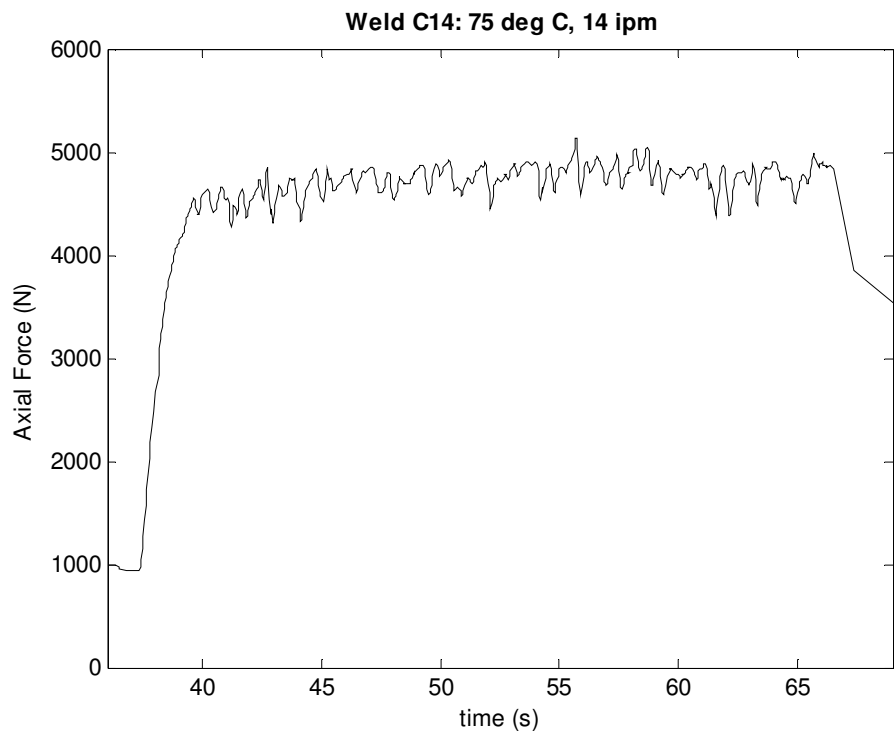
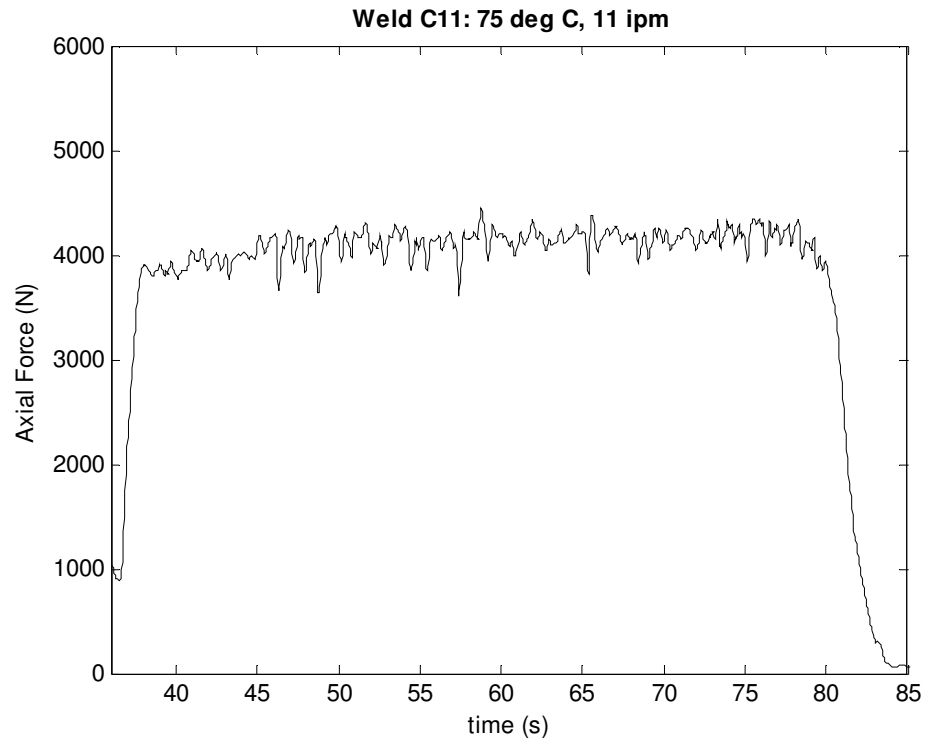


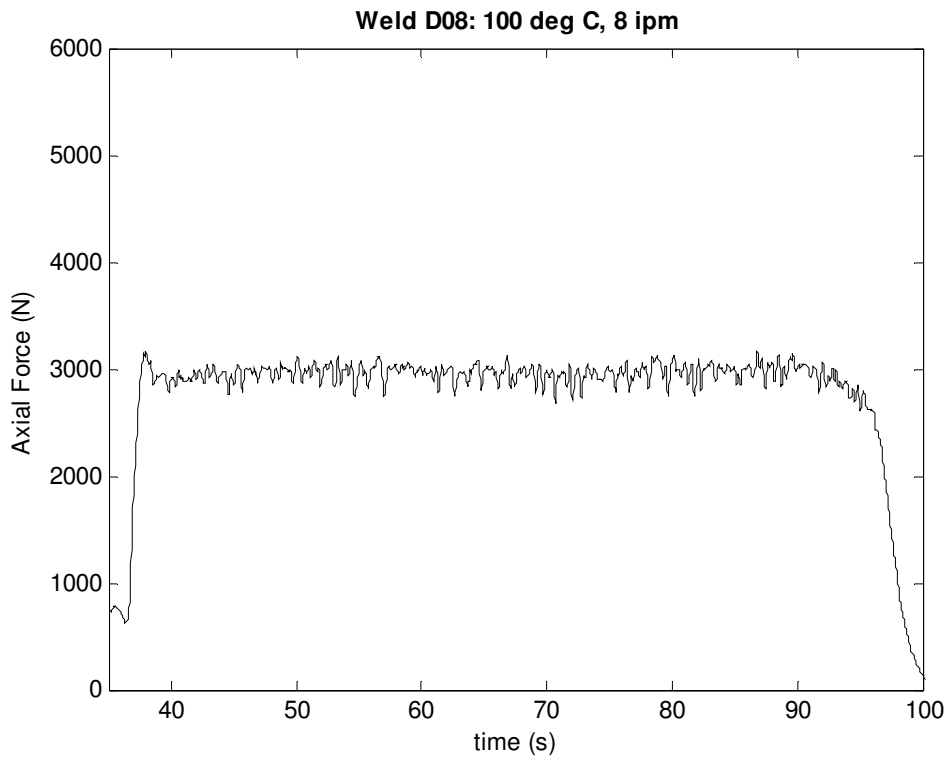
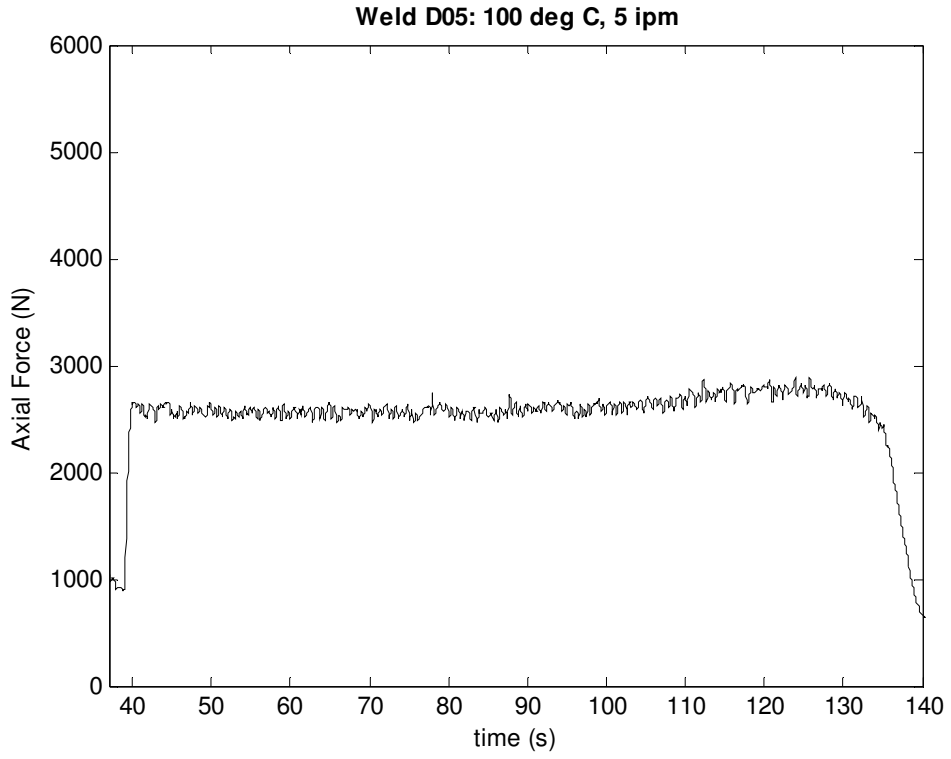


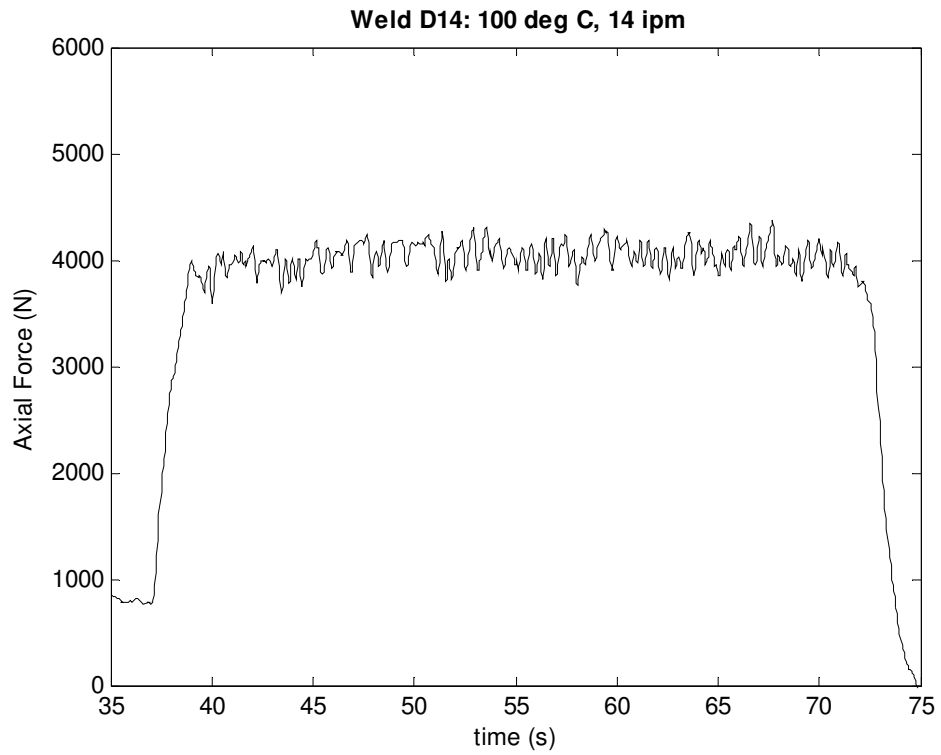
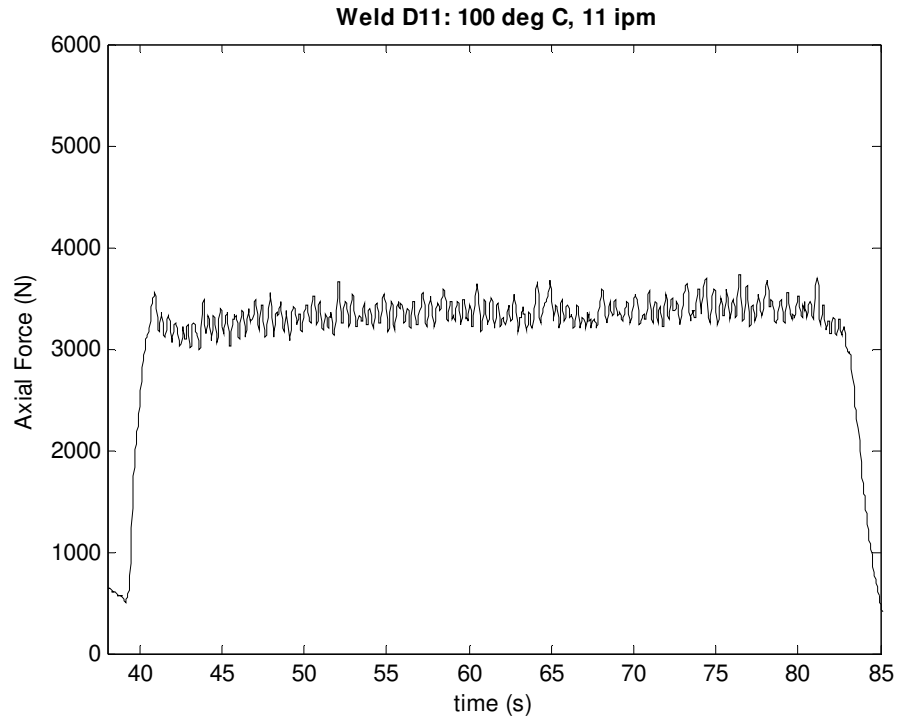


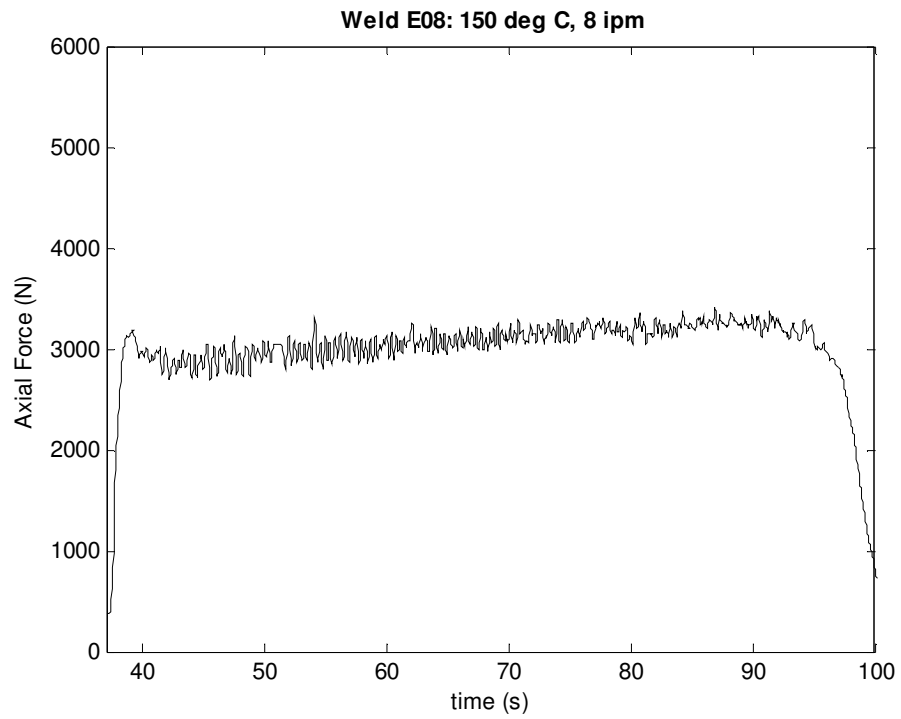
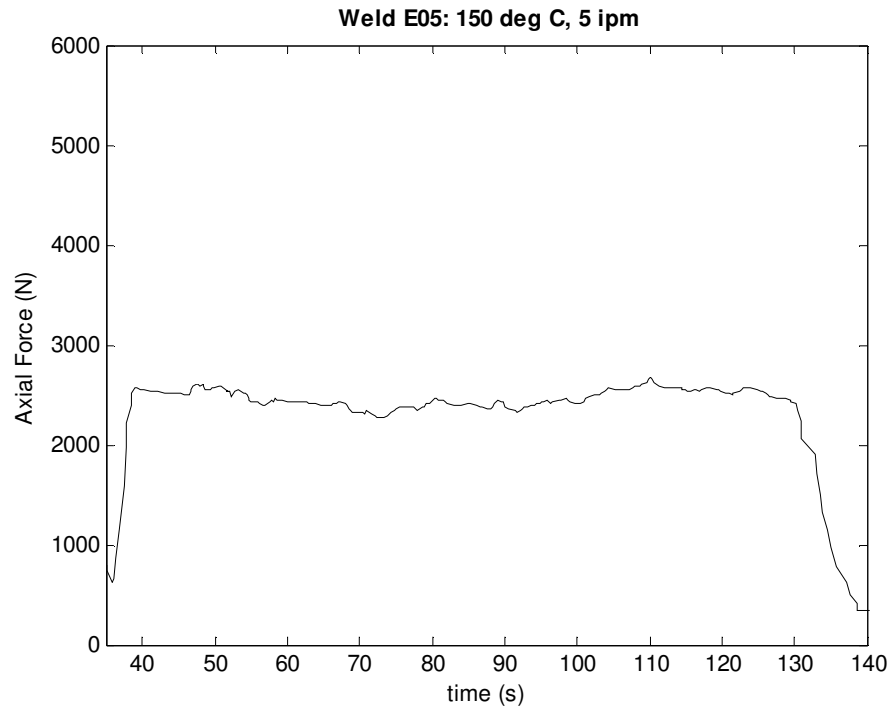




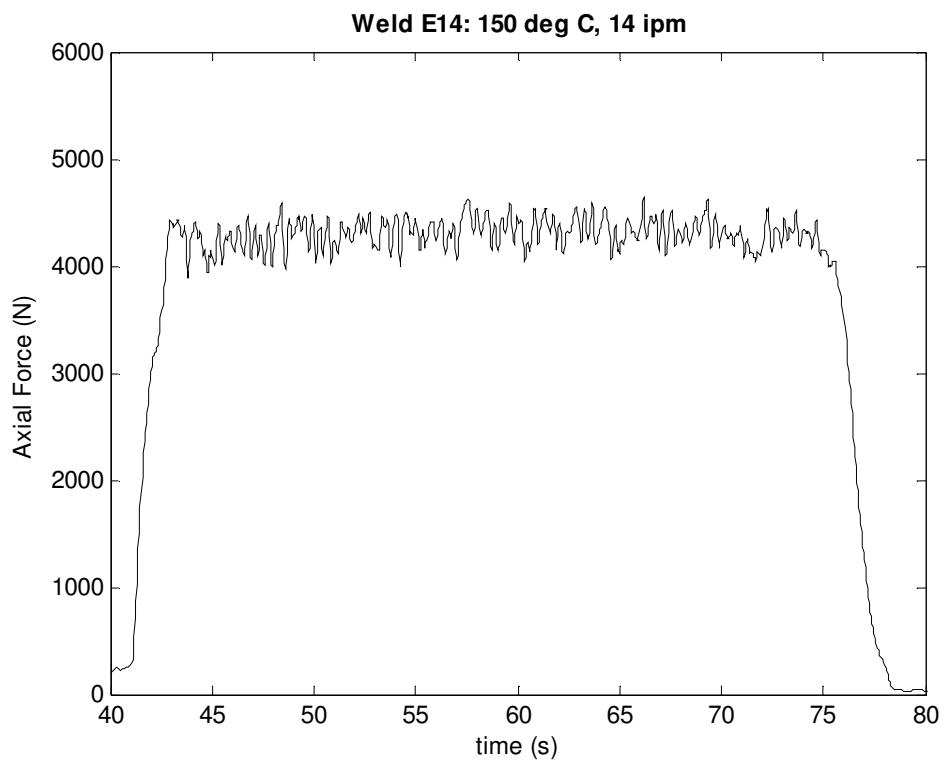
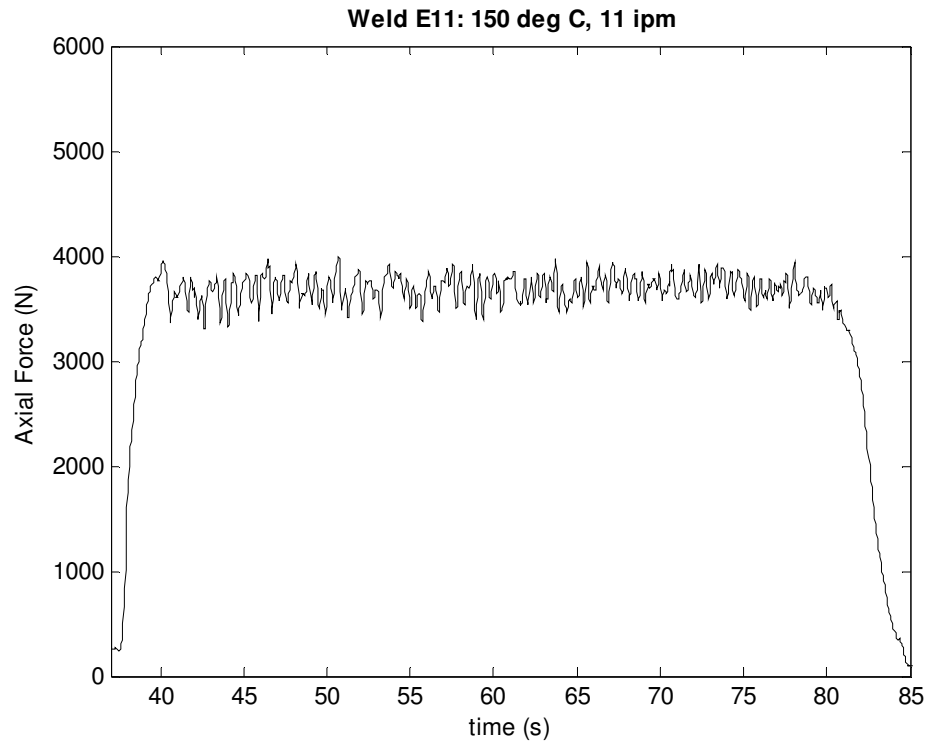


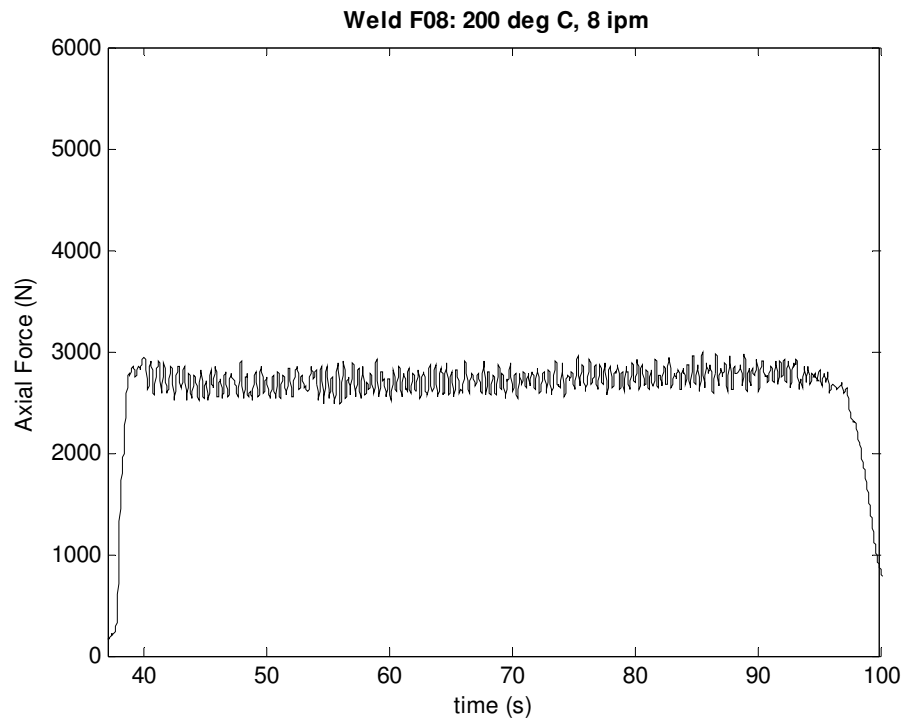
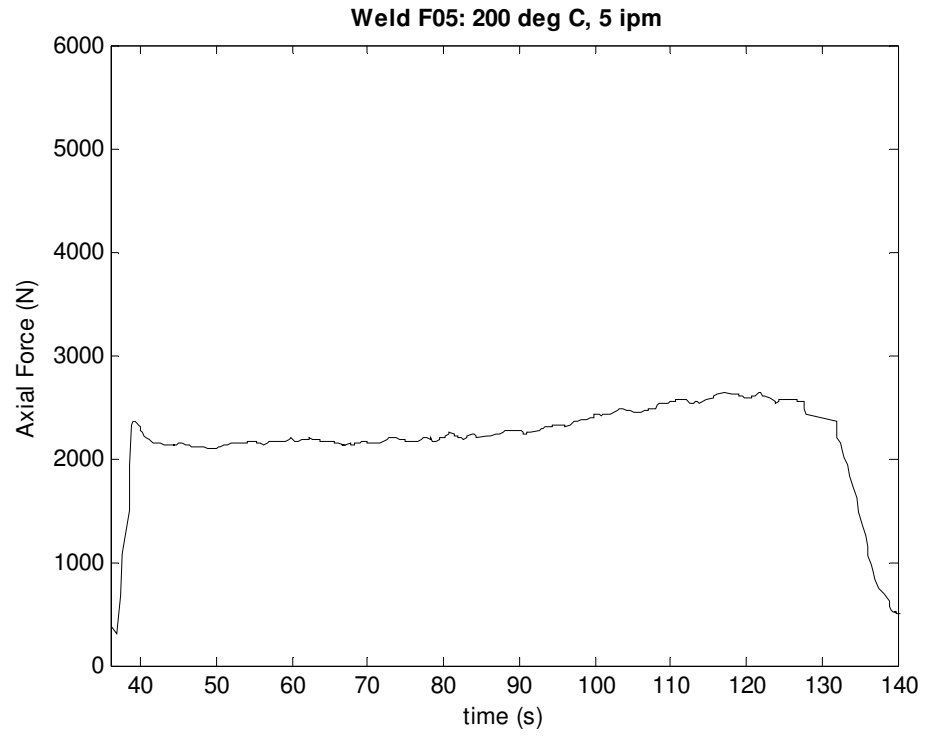


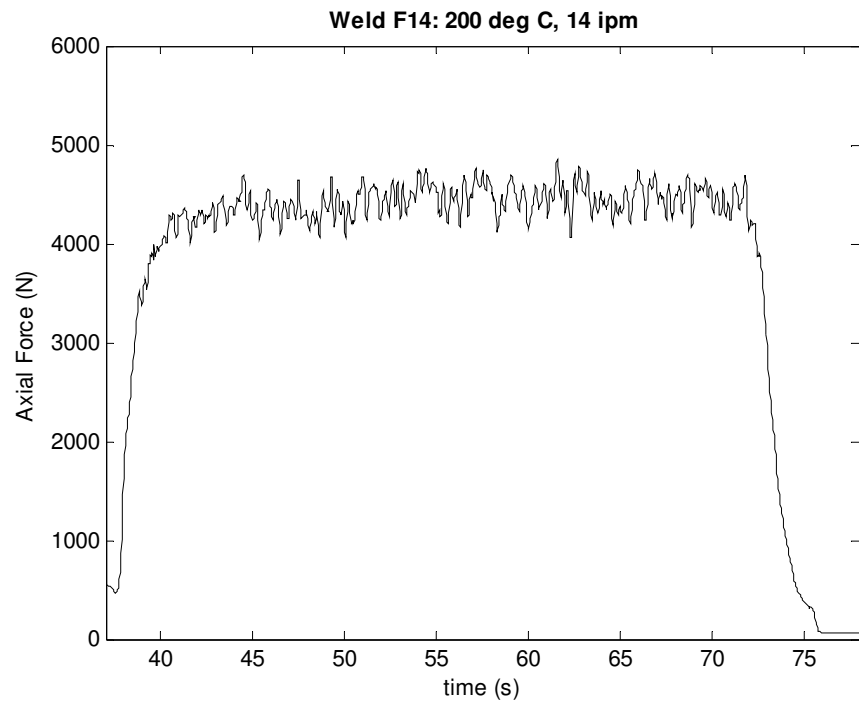
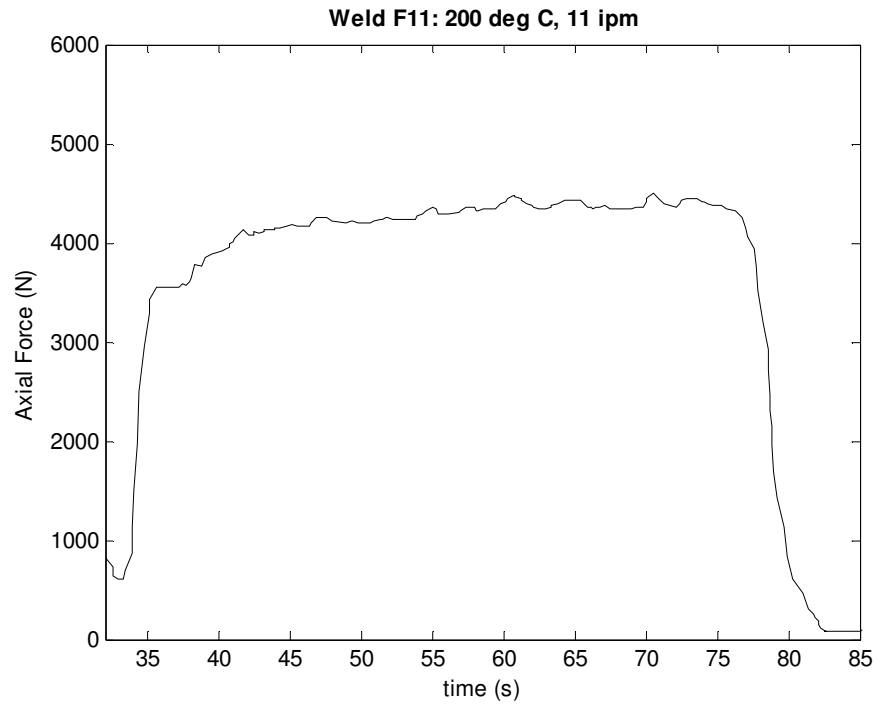


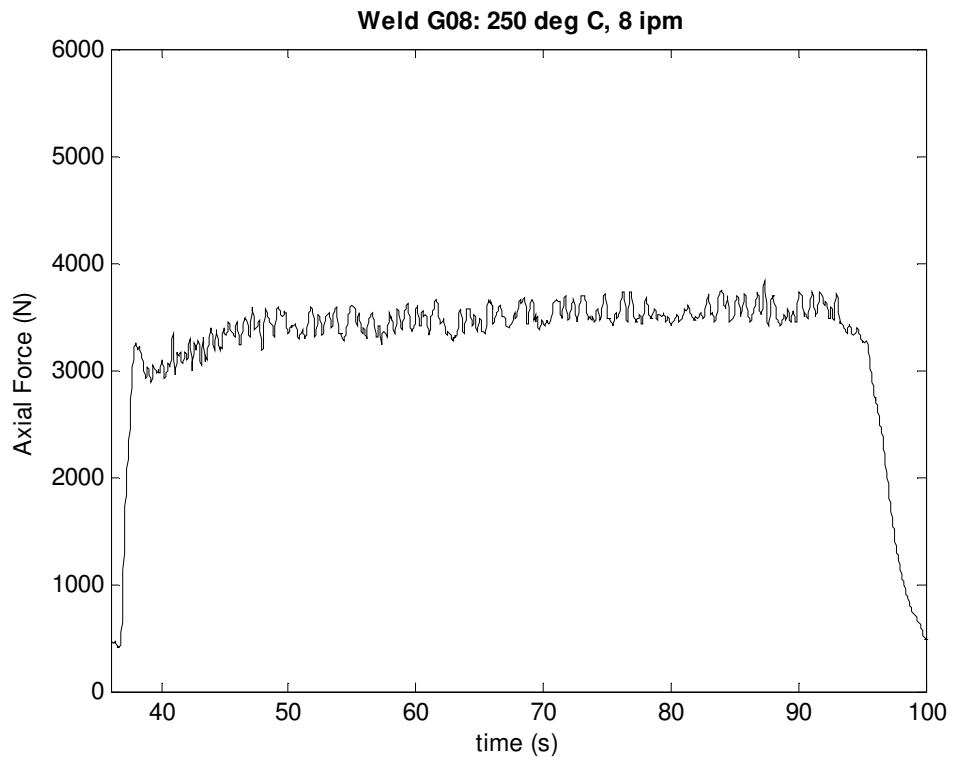
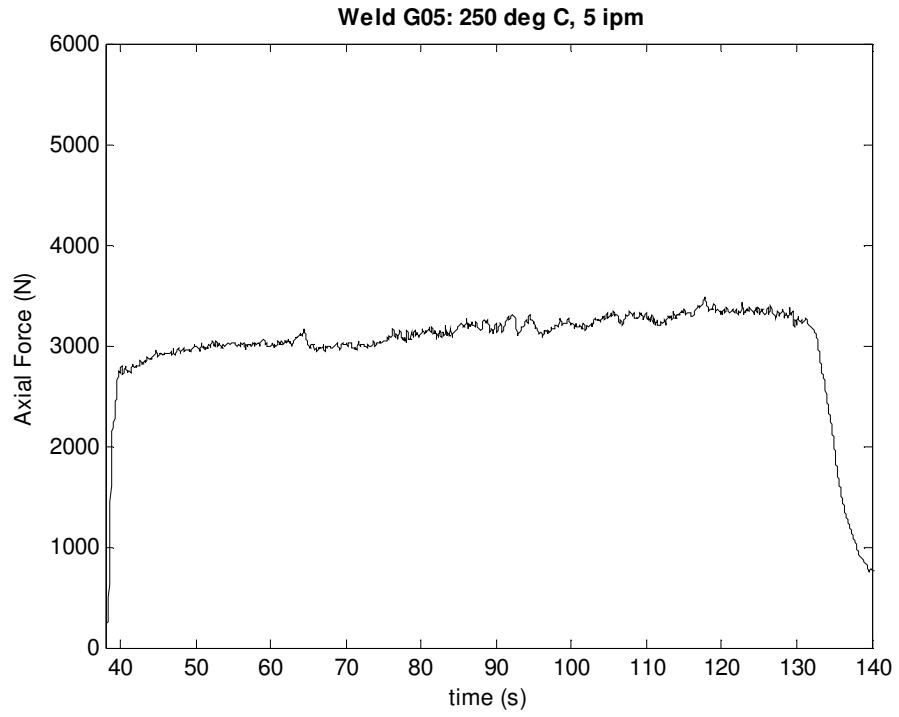


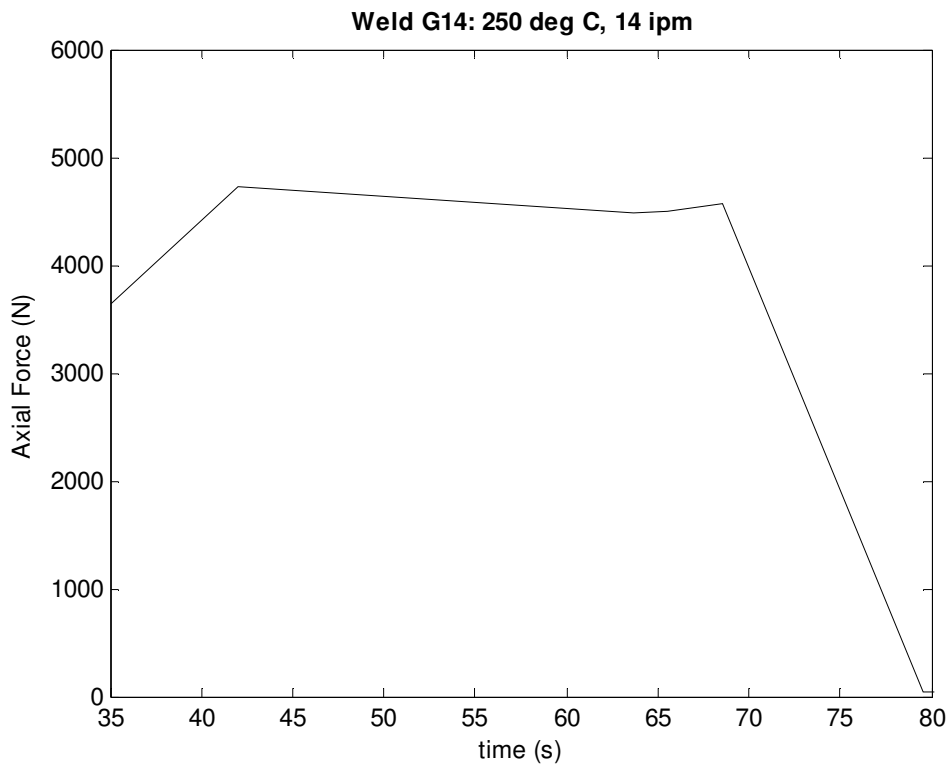
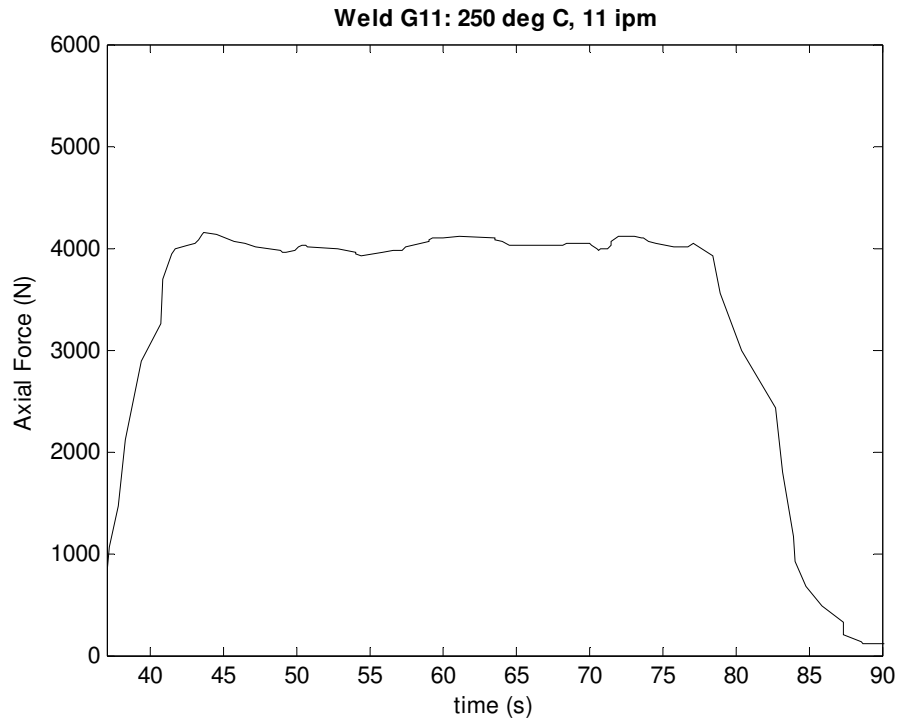


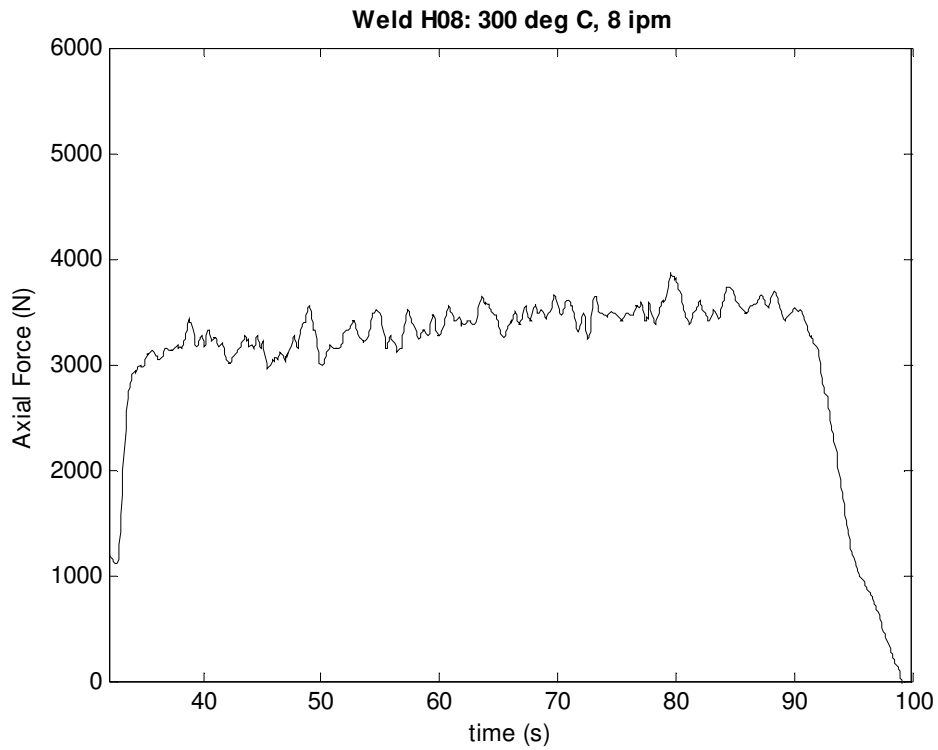
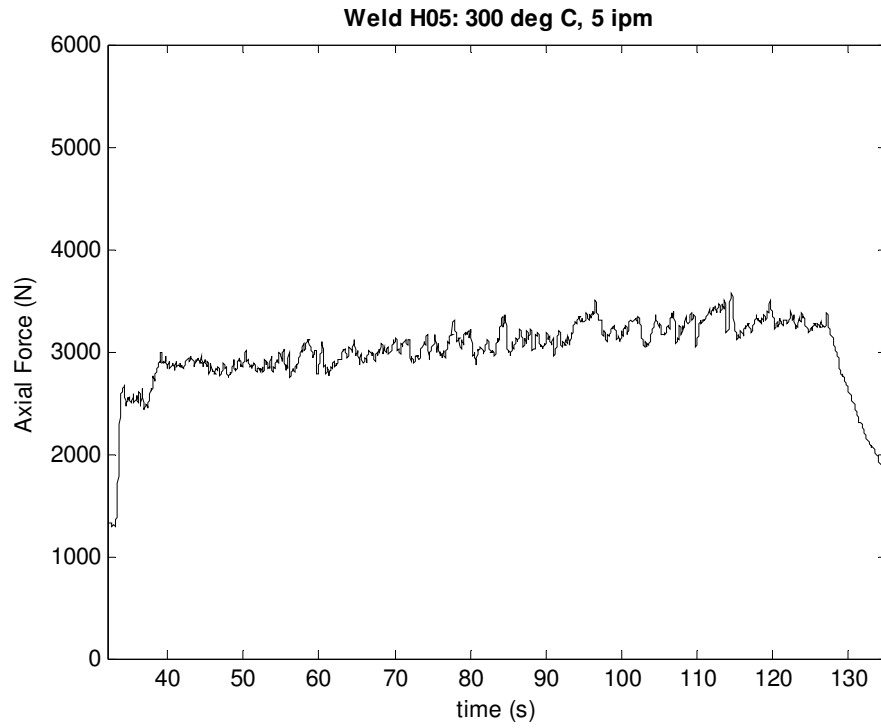


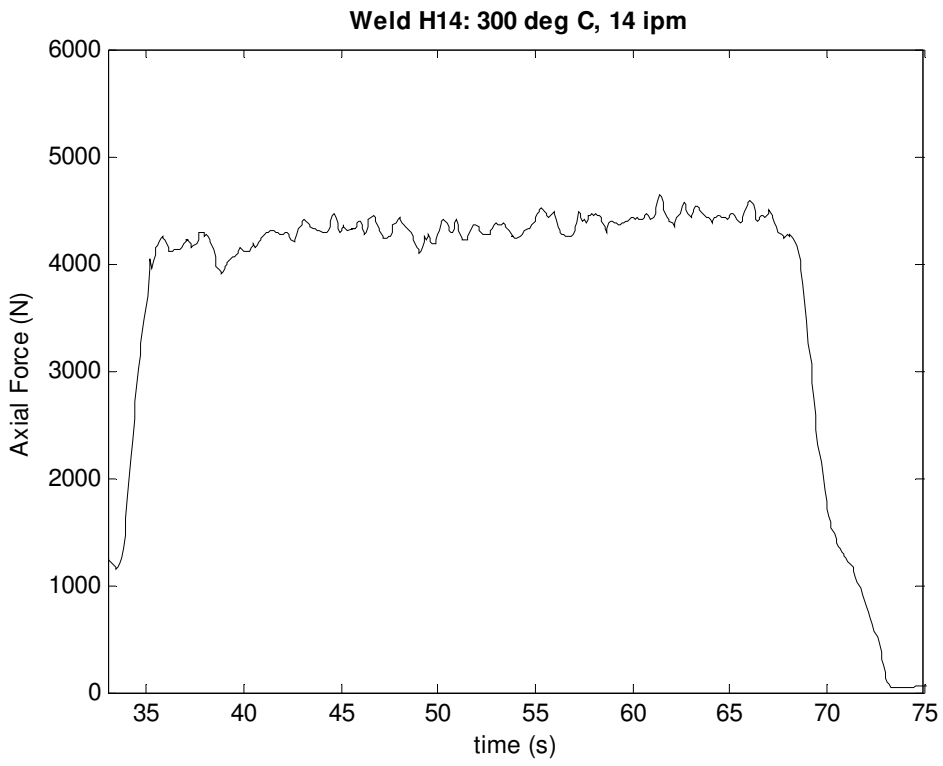
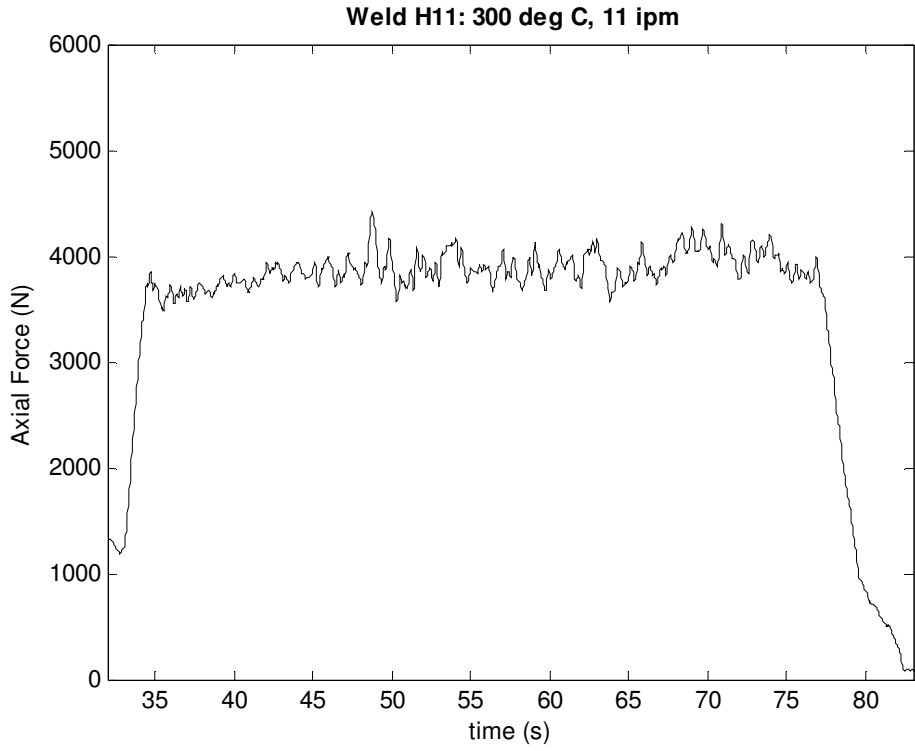












## References

- [1] Thomas, W. M., Nicholas, E. D., Needham, J. C., Murch, M. G., Templesmith, P., and Dawes, C. J. G.B. Patent Application No. 9125978.8 December 1991
- [2] Nandan, R., DebRoy, T., and Bhadeshia, H.K.D.H. “Recent Advanced in Friction Stir Welding – Process, Weldment Structure and Properties.” Progress in Materials Science Vol. 53, No. 6 (2008): 980-1023
- [3] Shtrikman, M. M. “Current state and development of friction stir welding Part 3. Industrial application of friction stir welding.” Welding International. Vol. 22, No. 11 (2008): 806-815
- [4] Frigaard, O., Grong, Ø., and Midling, O.T. “A process model for friction stir welding of age hardening aluminum alloys.” Metallurgical & Materials Transactions A. 32. (2001): 1189-1200
- [5] Ma, Z.Y. “Friction Stir Processing Technology: A Review.” Metallurgical and Materials Transactions A. Vol 39, Issue 3 (2008): 642-658
- [6] Balasubramanian, V. “Relationship between base metal properties and friction stir welding process parameters.” Materials Science and Engineering A. Vol 480, Issues 1-2 (2008): 397-403
- [7] Mishra, R. S., and Ma, Z. Y. “Friction stir welding and processing.” Materials Science and Engineering: Research Reports. 50 (2005): 1-78
- [8] Bernath, Jeff. Personal Communication. 7 November 2008. <jbernath@ewi.org>
- [9] Colegrove, P. A., and Shercliff, H. R. “Development of Trivex friction stir welding tool (Parts 1 and 2).” Science and Technology of Welding and Joining. Vol. 9, No. 4 (2004): 345-361
- [10] Crawford, Reginald. “A Mechanistic Study of the Friction Stir Welding Process.” Dissertation, Vanderbilt University. August 2006.
- [11] Cabage, Bill. “New way to weld.” Oak Ridge National Laboratory Reporter. No. 84 (2006).
- [12] Palm, Frank. “Laser supported friction stir welding method.” United States Patent 6,793,118. September 2004.
- [13] Kou, S., and Cao, G. “Arc-enhanced friction stir welding.” United States Patent 7,078,647. July 2006.



- [14] Grant, G. J., Khaleel, M., Eberhardt, J. J., Arbegast, B., Stone, G., Howard, S., and Allen, C. "Friction stir joining and processing of advanced materials including MMCs." High Strength Weight Reduction Materials. (2005): 112-121
- [15] Suzuki Riichi, Takahashi Takehiko, Hioki Susumu, Yamamoto Naoki, and Kaneko Yuuta. "On pre-heating effect for friction stir welding of aluminum alloy – A feasibility study of friction stir welding with heating of aluminum alloy (Report 1)" Quarterly Journal of the Japan Welding Society. Vol. 24, No. 3. (2006): 281-286
- [16] MatWeb Material Property Data. 2008. MatWeb. 14 November 2008.  
<<http://www.matweb.com>>
- [17] Kumar, K., and Kailas, S. V., "The role of friction stir welding tool on material flow and weld formation." Materials Science and Engineering A. Vol. 485 (2008): 367-374.
- [18] Sellars, C.M., and Tegart, W.J.M. "Hot Workability." International Metallurgical Reviews. No 17 (1972): 1-24
- [19] Nandan, R., Roy, G. G., and Debroy, T. "Numerical Simulation of Three-Dimensional Heat Transfer and Plastic Flow During Friction Stir Welding," Metallurgical and Materials Transactions, Vol. 37A, (2006): 1247-1259
- [20] Simar A., Pardoen T., and de Meester B., "Influence of friction stir welding parameters on the power input and temperature distribution on friction stir welding." Proc. of the 5th International Symposium on Friction Stir Welding. (2004).
- [21] Simar A., Pardoen T., and de Meester B. "Effect of rotational material flow on temperature distribution in friction stir welds." Science and Technology of Welding and Joining, Vol. 12, No. 4 (2007): 324.
- [22] Santiago D.H., Lombera G., and Santiago U. "Numerical modeling of welded joints by the friction stir welding process." Materials Research, Vol. 7, No. 4. (2004): 569.
- [23] Pew J.W., Nelson T.W., and Sorensen C.D. "Torque based weld power model for friction stir welding." Science and Technology of Welding and Joining. Vol.12, No. 4 (2007): 341.
- [24] Russell M.J., and Shercliff H.R. "Analytical modeling of microstructure development in friction stir welding." Proc. of the 1st International Symposium on Friction Stir Welding. Session 08, (1999).

- [25] Milding O.T., and Grong O. "A process model for friction welding of Al-Mg-Si alloys and Al-SiC metal matrix composites"; Acta Metall. Mater. Vol. 42, No. 5 (1994): 1595.
- [26] Frigaard O., Grong O., Bjorneklett B., and Midling O.T. "Modelling of thermal and microstructure fields during friction stir welding of aluminium alloys." Proc. of the 1st International Symposium on Friction Stir Welding. Session 08, (1999).